DOI: 10.1111/cgf.14209

COMPUTER GRAPHICS *forum*
Volume 40 (2021), number 6 pp. 135–161

Visualization of Tensor Fields in Mechanics

Chiara Hergl,[1] Christian Blecha,[1] Vanessa Kretzschmar,[1] Felix Raith,[1] Fabian Günther,[2] Markus Stommel,[3] Jochen Jankowai,[4] Ingrid Hotz,[4] Thomas Nagel[5] and Gerik Scheuermann[1]

[1]Leipzig University, Leipzig, Germany
blecha@informatik.uni-leipzig.de,kretzschmar@informatik.uni-leipzig.de,raith@informatik.uni-leipzig.de,scheuermann@informatik.uni-leipzig.de
[2]TU Dortmund University, Dortmund, Germany
fabian.guenther@tu-dortmund.de
[3]Leibniz Institute of Polymer Research Dresden, Dresden, Germany
stommel@ipfdd.de
[4]Linköping University, Linköping, Sweden
jochen.jankowai@liu.se,ingrid.hotz@liu.se
[5]Technische Universität Bergakademie Freiberg, Freiberg, Germany
thomas.nagel@ifgt.tu-freiberg.de

Abstract

Tensors are used to describe complex physical processes in many applications. Examples include the distribution of stresses in technical materials, acting forces during seismic events, or remodeling of biological tissues. While tensors encode such complex information mathematically precisely, the semantic interpretation of a tensor is challenging. Visualization can be beneficial here and is frequently used by domain experts. Typical strategies include the use of glyphs, color plots, lines, and isosurfaces. However, data complexity is nowadays accompanied by the sheer amount of data produced by large-scale simulations and adds another level of obstruction between user and data. Given the limitations of traditional methods, and the extra cognitive effort of simple methods, more advanced tensor field visualization approaches have been the focus of this work. This survey aims to provide an overview of recent research results with a strong application-oriented focus, targeting applications based on continuum mechanics, namely the fields of structural, bio-, and geomechanics. As such, the survey is complementing and extending previously published surveys. Its utility is twofold: (i) It serves as basis for the visualization community to get an overview of recent visualization techniques. (ii) It emphasizes and explains the necessity for further research for visualizations in this context.

Keywords: scientific visualization, visualization

1. Introduction

Tensors are one of the fundamental data types taught in basic visualization classes and appear in many application areas because they provide a generic concept for multiple physical theories. Thereby, their physical interpretation and their mathematical properties are versatile, e.g., they can appear as descriptors for multilinear relations of different order, as derivatives of vector fields, or describe anisotropic material properties. Hence, even more than for scalar or vector fields, visualization methods for tensors of higher-order are most frequently developed for specific settings. Some of them are easily transferable, while others are not.

Thus, tensor field visualization comprises several different perspectives: (i) the mathematical definitions and properties, (ii) visualization concepts ranging from general-purpose to specific methods, and (iii) the application-specific context including the semantics of the tensors and typical related research questions. In this survey, tensor field visualization is discussed from all these perspectives with a strong emphasis on the application in structural mechanics, biomechanics, and geomechanics, which also distinguishes it from previous related surveys. All these areas are based on the same concepts of continuum physics and are correspondingly closely interconnected. This survey highlights the usefulness of tensor analysis as well as the need for novel visualization methods in these areas. It shows their commonalities and their essential differences. This work is restricted to tensors of order two and higher since tensors of order zero (scalars) and one (vectors) have been covered frequently. The most prevalent second-order tensors in the considered fields are stress, strain, and orientation distribution tensors. However, also

tensors of higher-order, like elasticity, play an essential role. Since tensors can also be interpreted as a set of representative scalar and vector fields, for example, eigenvectors, eigenvalues, or other invariants, the survey also touches on the visualization of multivariate data. Concerning biomechanics, diffusion tensor imaging (DTI), or high angular resolution diffusion imaging (HARDI) is not discussed because they are summarized in their own surveys, and they focus on other questions than the ones coming from continuum physics.

The structure of the survey reflects the different perspectives on tensor visualization. First, the creation of the survey, the application areas with their common visualization techniques used by domain experts, and common research questions are described. A table gives an overview of the covered techniques, theories, and applications. The mathematical background, necessary to understand the most commonly used tensors and their properties in the applications, is introduced in Section 3. Sections 4 to 9 summarize techniques that are categorized as glyphs, geometry- or texture-based methods, topological feature visualizations, or multivariate data techniques. Section 10 captures specific challenges related to tensor visualization and the differences between the application areas as well as discusses open questions. It also entails a brief description of possible future research directions regarding the reviewed paper base (see Table 1). Finally, Section 11 gives a short conclusion. To sum up, the main contributions of the survey are:

- Summary of visualization methods used in structure-, bio-, and geomechanical applications,
- Analysis of the recent development in tensor field visualization, and
- Identification of underrepresented areas.

Scope

Tensor visualization appears in many application areas. Consequently, there already exist related surveys, and some overlap is inevitable. The closest related survey on tensor visualization was written by Kratz et al. [KASH13]. A survey about tensors in image processing and computer vision [CnMMM*09] also covers many of the basic tensor visualization methods. Since these two surveys, a lot happened in the area, and novel trends in the field emerged, which is summarized in our work (see Section 11). Nevertheless, this survey contains all information to understand the presented methods, which means that some key works covered by previous surveys are also included.

In terms of surveys with a different focus but shared points of interest, there exists a report on topological visualization [HLH*16] that also touches on tensor field topology. A survey about visualization in material science [HS17] deals with a similar application area but does not focus on tensor fields. The most recent survey on the visualization of tensor fields by Bi et al. [BYDS19] is restricted to streamline and glyph-based methods focusing on DTI data.

The targeted audience of this survey are experts in visualization looking for a summary of new works, those who search challenging questions to work on, and beginners in the field who want to get an overview of recent tensor visualizations in structural mechanics, bio-, or geomechanics.

Procedure of writing this report

The paper collection process started with the choice of the leading visualization conferences and journals: The IEEE Visualization Conference (IEEE Vis), the EuroVis conference, the IEEE Pacific Visualization Symposium (PacificVis), the IEEE Transactions on Visualization and Computer Graphics (TVCG), and the Computer Graphics Forum (CGF). Since our report constitutes a follow up to the state-of-the-art report [KASH13], all papers published in these conferences and journals since 2013 and many papers of domain-specific conferences and journals were reviewed. All papers containing any of the following keywords: *Tensor*, *Matrix*, *Stress*, *Strain*, *Multilinear*, *Multivariate*, or *Multidimensional* in their metadata or content have been further inspected.

From the papers published in the IEEE TVCG (IEEE Vis) since 2013 (incl.) (2327 publications), 367 publications were marked as possibly relevant. From the 432 publications at PacificVis since 2013 (incl.), 90 publications remained. In CGF almost 2000 papers were published, and 371 papers were issued at EuroVis since 2013 (incl.). Filtering this set lead to 1264 of the 2000 publications. For visualization methods of tensors in biomechanics, about 200 publications from the Visual Computing for Biomedicine conference (VCBM) during the last 13 years have been investigated. The number of hits for the above keywords was below 5. Each of the remaining publications has then been worked through and rated according to its relevance. Simultaneously, a graph has been designed with papers as nodes and citations as edges. In a second phase, this graph has been gradually expanded with the references or citations of the first extraction round papers. Thus, also domain-specific works and those from other conferences and publishers found their way into the paper pool. This process was repeated again and again, resulting in a set of papers that hopefully gets close to completeness for publications related to the visualization community and gives a representative selection in the application areas. In the end, the graph had more than 3550 nodes where about 3240 were marked as not relevant or not accessible (due to missing access licenses). About 300 papers were marked as interesting, e.g., they contain for this survey relevant keywords, the application matches or the visualization can perhaps be carried over to the treated applications, in the first review. About a third of the papers have been presented and discussed for relevance in a sub-group of the survey authors. This lead to about 120 remaining papers for this report coming from the graph. Each relevant paper has also been summarized in a few sentences to distill the survey's final content.

During this analysis, it has been recognized that, even though most of the common tensors in all applications share their physical meaning, the structure of the fields and the visualization approaches differ a lot.

2. Application Domains from a Visualization Perspective

The following section describes the selected application areas: structural mechanics, bio-, and geomechanics. In all these domains we find applications dealing with designing and understanding material properties, designing structures, and understanding the behavior of structures and materials under load. Data is collected or generated by simulations, imaging, observations, and experiments.

Table 1: *Distribution of reviewed publications of the focused application areas over different visualization techniques.*

Methods/Concepts		Glyphs/Hedgehogs	Textures	Line-/ Geometry-based	Topology/ Feature-based	Hybrid/ Volume Methods	Exploration/ Attribute space	Introduction to
Domain	Tensor type							
Structural Mechanics	Generic	[KAH14] [SK10b] [JKM06] [HFH*04]	[FHHJ08a]				[OP14] [Car14] [War02]	[KASH13] [KYHR05] [Wri08] [Hol00] [DT06]
	Stress/Strain from (dense) simulations	[MBH*08] [Hab90] [MSM96] [PL20]	[SSK*14] [Mol18] [KKH11] [BES15] [SLZZ15] [HFH*06]	[KGSS20] [WWW20] [DH93] [KSZ*14] [SKZ*15] [SSK*14] [LZY*17] [AJL*19] [KLC16] [FWB03]	[ZGZ17] [Gao18] [LBHL97] [LLH97]	[KMH11] [FH15] [CRBC04]	[RBN*19] [KMH11] [KMH11]	[Hab90] [WH05] [KGM95]
	Orientation Distribution	[WAS*18] [JKLSI10] [JKM06] [ZSS15] [MB15]				[WAL*14] [BHA*15] [BWW*17]		[DT06]
	Elasticity	[BB01] [BL14] [ZTL13] [NBJ*08] [JFK*15]						[HNS20]
	Uncertainty Tensor	[AWHS15] [GRT19]						
	Others	[ZSS17]						[Bra03] [Dan18]
Biomechanics	Generic		[EHHS12]					[AAC*19] [Hum03] [Wol93] [PJB*96] [PSB10]
	Stress/Strain from (dense) simulations	[RDMM12] [WBWD12] [SBWK01] [WY03]	[WAWS17] [ZP02] [SEHW02] [WBWD12] [WLY04] [KASH13]	[WLY04]	[WLY04]	[TNKW20] [SEHW02] [WLY04]		[NK12] [KNB13]
	Stress/Strain from imaging	[SCK*16] [WBT*14]				[DGBW10] [SCK*16] [SCRFSSRA09]	[WBT*14] [CA17] [SCK*16]	
	Orientation Distribution	[NK12] [WK14] [ZFD*14] [GYLG20] [SSSSW13] [LNY*18] [EKH*04] [SS08] [LAK*98] [Kin04] [SK10a]	[FHHJ08a] [HS05] [LAK*98]	[GDMS*15] [GYLG20] [LNY*18] [DSB*19] [HS05] [SP04] [WKL99]		[KWH00] [HWS*19] [TIHN07] [HWA*09] [JDL09] [KW99] [ZDL03]	[Wan04] [WH07] [WV04] [ZTW06]	[GDMS*15] [HWS*19] [BHC*19] [VZKL06] [FL96]
	Elasticity	[HNKS19] [KDL*20] [MSP16]						
	Other							[BML94] [LBMP*01]
Geomechanics	Generic	[NJP05]	[RASS17]				[RSA*18] [RMH*18]	[KHvdH99]
	Stress/Strain	[FKGR03] [LLP*18] [HYW03]	[HFH*04] [HFH*05]	[JSF*02] [BP98] [HYW03] [SFH*01]	[CRB*05]			[KHvdH99] [RGBN14]
	Moment Tensor	[BDLG15] [BUM*12] [LGSWN14] [WGSC18] [CL12] [CUS*15] [LH07] [DP08] [LYC*14] [GD11] [Nee04] [Boy18] [UBG*12] [ASKT18] [UBGB10] [YVAB18] [ZYZ*19] [Wil93]						[Cro04] [Gil71] [HPR89] [KR70] [RJ89] [TT12] [TT15] [Vav14]
	Higher-Order							[Hel15] [Bac70]
	Others					[OBH*11]	[BRS*19] [BRP*20] [RBR*20]	[SJCT20]
Other application		[BH04] [BN03] [GRT17] [SK16]	[BW03] [CL93] [DR00] [SKJY06]	[ASNZH11] [Ben04]		[CZMB*09]		[AFPA06] [CAA01] [CEW*08] [SWBG06] [dLGALW09] [EK06]
Universal		[KASH13] [FHHJ08b] [KW06] [SK10b] [KAH14] [War02] [GRT19] [Bar81] [SHB*99] [SYI*97]	[HFH*04] [ZP03a] [ZP03b] [HES04] [BH17] [ASKH12], [KASH13] [ZDL*11] [VKP00]	[Dic89] [DH92] [WB05] [WWW20] [ACSD*03]	[HLH*16] [WPG*97] [PYW*16] [DH94] [Sch11] [ZP04] [THBG12] [ZPP05b] [PYW*13] [ZTZ15] [ZZ15] [RKZZ19] [ZS18] [ORT18] [PMC*16] [PRK*17] [RKG*17] [Tri02] [Aue13] [WH17] [JWH19] [ZP05] [PLC*11] [AKK*13] [LYLZ12] [ZRH14] [ZRH15] [ZRSZ18] [KRZ*19] [QRZZ20] [Del96] [RC06] [SNAHH11] [TKW08] [TSHC01] [ZHT06] [ZPP05a] [ZTP06] [ZYLL08]	[ZMB*03]	[RBN*19] [DLL11] [CNCO17] [WZL*12] [JH18] [MH19] [JSJ*20]	[HLL97] [KST*10] [Lan12] [LW08] [MB06] [MJM*06] [PFA06] [WH05] [YM08] [HBGW20]

The intention of this section is not to provide an exhaustive overview but to highlight exemplary areas, which have been in the focus of visualization applications. It also summarizes visualization practices in the communities, mainly basic methods, e.g., plotting and coloring of surfaces. Most simulation tools, for example, Abaqus [HKS98], NX (Siemens) [Sie20], and ANSYS Mechanical [SNY18], in structural engineering, provide some visualizations. Also, analysis tools, like Paraview [Aya15], or self-written tools using, for example, MatLab [HH00], are used. In the field of biomechanics, one can find a larger variety of more specialized visualization tools often developed in individual research projects.

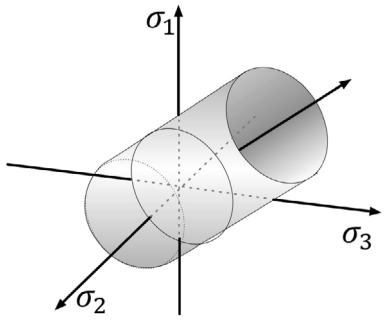

Figure 1: *Yield surface in the principal stresses spanned by the three eigenvalues σ_i of the stress tensor. Points inside the surface represent an elastic state of the material, points on the surface indicate plastic behavior, and points outside the surface are not permitted.*

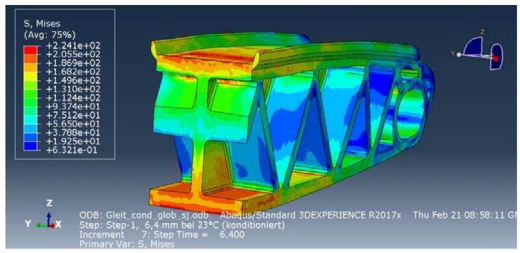

Figure 2: *A typical visualization of the distribution of the von Mises stress generated with the software Abaqus [HKS98].*

2.1. Structural mechanics

Structural mechanics is a field of applied mechanics. It is concerned with the computation of deformations, forces, stresses, and strains within a solid material or structure [Dog00, Hol00]. A typical goal is the design of efficient load-bearing structures facilitating novel lightweight material. An essential step thereby is the evaluation of the structure's performance in terms of strength, flexibility, or responses to loads. Important quantities for such analysis are stress and strain tensors which in conjunction with a chosen failure model give insight into the structure's properties. Tensors are also used to describe material properties, e.g., the fiber orientation tensor for fiber-reinforced material. In this context data from numerical simulations are prevalent, however, also experiments and imaging generate large amounts of multivariate data including tensor fields as essential entities. Within the broad field of structural mechanics, we will focus on three topics related to the design of functional parts: (i) *Stress tensor analysis of load-bearing structures*, (ii) *Fiber orientation tensor describing complex materials*, and (iii) *Tensor comparison for structure topology and shape optimization*. Visualization plays an important role in understanding the stress distribution in its relation to the material and geometry. Specifically it addresses the following topics:

- Designing components by visualizing force paths in materials,
- Comparing and evaluating different failure models for complex materials,
- Comparing performance metrics for different design options,
- Optimizing processes, and
- Detecting and analyzing critical areas in components.

Stress tensor analysis of load bearing structures – The analysis of critical areas during the design of load-bearing structures based on finite element simulations is a common task. Different models describe yield, damage, or material failure using scalar metrics derived from the stress tensor and the material properties. Yield criteria can be represented as surfaces in the space spanned by, e.g., the principal stresses (see Figure 1). Inside this yield surface, the material exhibits a (visco)elastic behavior, which becomes (visco)plastic upon reaching the yield surface. Diagrams, color plots, or isosurfaces are usually used to highlight critical areas in the structure (e.g., [ZMD19]). Figure 2 shows a rendering of the von Mises stress, a scalar metric used as yield criterion for isotropic and ductile metal.

Fiber orientation tensor describing complex materials – This application scenario is concerned with the analysis of properties of anisotropic composite materials, e.g., fiber-reinforced polymers, which play an increasing role in high-tech industrial products [Slo11]. The properties of such materials are largely determined by specific topics, like the fiber orientation and length distribution [FL96]. One approach to predict the fiber distribution is the simulation of the injection molding process. Deriving material properties from the fiber orientation is a complex task, and a careful evaluation of the simulation results is essential [DT06, ZSS15]. Another source enabling the reconstruction of fiber orientation distributions is found in three-dimensional X-ray computed tomography (X-CT) [MPB*14]. The results are highly resolved three-dimensional imaging data. Extracting the relevant characteristics, e.g., the orientation tensors, requires advanced image analysis and visualization.

Tensor comparison for structure optimization – Designing optimal components is often an iterative process governed by computer-aided simulations. Optimization goals involve saving resources, like energy, weight, material, or time, while retaining the component's strength and load-bearing properties. An example is the design of light-weight structures that optimally support the load transfer in a component [SSK*14]. The comparison of design options, like geometry, material, and operating conditions, requires efficient methods to explore the correlation of design parameters and key performance metrics. Examples are the optimization of shell elements using rib layouts for lighter components [LZY*17] and the design of volumetric Michell Trusses [AJL*19].

2.2. Biomechanics

Biological tissues are in the center of most biomechanic applications. In general, these are anisotropic materials with a complex internal structure as in trabecular bone or fibrous constituents in cardiovascular tissues, etc. [NK13]. Biomechanics tries to understand the structure-composition-function relationships of the tissue (e.g., [GNK12]). Mechanobiology aims at understanding mechanisms of how the tissues adapt their composition and structure in response to mechanical and biophysical cues in a process called remodeling [AAC*19]. This knowledge is exploited to create biological substitutes in a process called tissue engineering [TNCK13]. This survey focuses on applications related to (i) bone architecture, (ii) cardiovascular tissues, (iii) cell structures, and (iv) fluid-structure interaction. Thereby as well the anisotropic tissues as the functional loads are expressed by tensors. Interesting data arises not only from simulations but also from diverse imaging methods. Visualizations can help to answer questions concerned with

- Relationships between bones (structure tensors) and function (stress tensors),
- Remodelling of soft tissues in response to loading, e.g., changes in structure, composition, and properties, and
- Fluid (wall shear stress)-structure interaction in, e.g., cardiovascular or respiratory systems.

Function and structure of bones, relation between structural and mechanical tensors – Bone architecture is known to be highly adapted to the mechanical loads experienced by the tissue [Wol93]. This link is so consistent that it even allows engineers to reverse the locomotion of animals that have been extinct for millions of years based on preserved trabecular bone structures [BHC*19]. To understand this anisotropic structure-function relationship, computational and experimental methods are used, resulting in data including tensors of various orders. Direct visualization of derived scalar fields can be found in related publications in the domain. E.g., to visualize the anisotropic stiffness of artificial lattice materials mimicking different types of bone Kang et al.[KDL*20] plotted effective elastic modulus surfaces in a three-dimensional space spanned by the lattices' unit cell axes. A similar approach was used to visualize fourth-order stiffness tensors derived from fourth-order structure tensors in [MSP16].

Fiber orientation tensor in cardiovascular tissues – The human heart has a complex geometry and structure with strongly varying muscle fiber orientations. Fiber structure distributions can be derived from experimental measurements (e.g., [WK14]). The most common visualization of fibrous or filamentous structures in the domain are hedgehogs representing their dominant alignment [NK13, KNB13, GM09]. To simplify the representation of the heart and improve the comparability, a standardized segmentation of the left ventricle has been introduced [CWD*02], which is frequently applied in visualizations [SCK*16]. Combined visualization of collagen fiber density and morphology was visualized in [HWS*19] using color plots and glyphs to illustrate the collagen network alignment characteristics.

Tensors describing the spatial organization of cells – The spatial organization of cells or nuclei with implications for tissue and tumor characterization can be described by structure tensors derived from images [ZFD*14]. They are often visualized as a field of ellipsoids. Also, computational models are used to study the dynamic remodeling of the cytoskeleton in response to mechanical signals [RDMM12]. In particular, the simulated polymerization and depolymerization of stress fibers are visualized using colored vector plots encoding their activation level and orientation (see Figure 3).

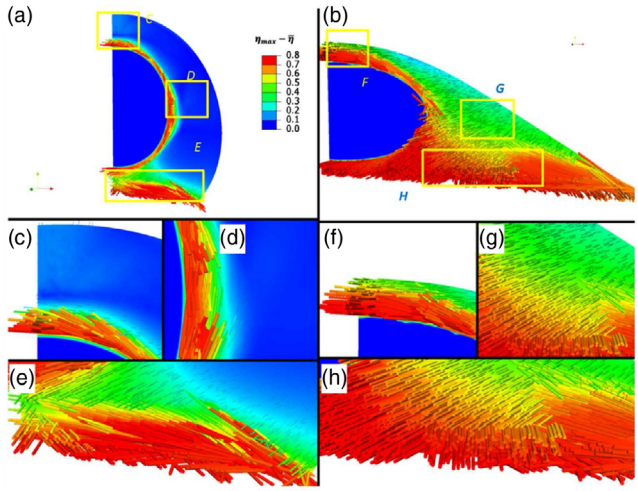

Figure 3: *Visualization of remodeling stress fiber network in a cell (cytoskeleton). The plot displays orientation and activation level (vector) of the stress fiber and the local variance (color) (image from [RDMM12]).*

Interaction of fluid-induced wall shear stress with tissue structures – The interaction of blood with vessel walls is another example of adapting tissues to mechanical loads. E.g., patient-specific mechanobiological frameworks are used to simulate the fluid-structure interaction and the growth of intracranial aneurysms. Often the results are visualized using surface coloring. In some cases, also vectorial hedgehog plots and streamlines used to illustrate the aneurism flow field can be found [TNKW20].

2.3. Geomechanics

In brief, geomechanics deals with the mechanics of soil and rock on a large variety of scales ranging from millimeters, e.g., the grain scale, up to the continental scale. Thereby, one goal is to understand the mechanical behavior of geo- materials under a wide range of conditions, e.g., considering drilling, building pipelines or bridges, accessing geo-reservoirs, or exploiting geological barriers. On a small scale, properties can be derived from experiments where the microstructure is captured by X-CT. From the images, deformations, strain, and arrangements of the constituting particles under controlled loading conditions can be calculated. On large scales, similar information can be estimated from seismic events, remote sensing, or other suitable methods. The derived results are an essential input for further simulations. Thereby, tensorial data is generated from simulations, observations, or experiments. Relevant tensors include the fabric tensors describing the orientation of particles or voids, elasticity tensors, deformation gradients, and stress

and strain tensors. Visualization and data analysis in geo- mechanics dealing with the above materials address a wide range of topics:

- Understanding of processes and prevailing conditions in the subsurface related to seismic moment tensors,
- Investigation, prediction, and effects of seismic events, and risk assessment in the context of geohazards,
- Localization and exploitation of reservoirs containing various resources (materials or energy), and
- Evaluating the properties of geomaterials from imaging.

Seismic moment tensor – During seismic events (earthquakes, landslides, or explosions), elastic strain energy is released and propagates or dissipates as seismic waves, heating, or fracture propagation along faults. Seismic waves can be recorded by seismometers even at a great distance, providing valuable information about the structure in the interior of the earth and the source of the event. In evaluating recorded data, the moment tensor plays a central role [Gil71]. It describes force couples acting on points on a fault and represents the moments generated by the seismic event according to a point source model. The moment tensor depends on the source and the fault. Its components are obtained from nine sets of so-called vector couples. The data sets generated are, in general, sparse and often incomplete, limited to a few locations along faults. Moment tensors are commonly visualized using plots [KR70, HPR89, TT12] or glyphs [Cro04] and are, e.g., used to investigate earthquakes.

Multi-variate data from tectonic simulations – Besides seismic observations of the earth, 3D models to simulate and visualize flows within the earth's mantle are developed. Such simulations contribute to understanding the earth's interior in time and length scales ranging from atomic size to the globe. This includes the simulation of earthquakes and the earth's crust's response [KHvdH99]. Other examples are numerical simulations investigating the viscoplastic flow of tectonic plates responsible for the plate deformations at subduction zones. Thereby, geological observations are used as constraints [RGBN14]. Many of these applications also involve tensor fields, e.g., postseismic stresses at faults.

Imaging of geomaterial – The scales knowledge derived from imaging is coupled with simulations for geological predictions. Imaging techniques are used to characterize the structure of geomaterial, estimate its physical properties, and finally understand the appearance of microcracks and voids. An example is the use of X-CT to quantify fabric in a polymer-bonded frictional granular material. Analyzing its constituents' relative orientation, described by fabric tensors, allows for a systematical structure characterization [SJCT20]. Such knowledge can then be exploited in numerical simulations, e.g., to assess the stability of dams [RBM20] or waste reservoirs [MGV*17, RBR*20].

2.4. Classification of the reviewed papers

Table 1 illustrates the used techniques and tensors grouped by the three different application domains. For each of the domains, the rows specify the common tensor types. Works without a specific application were sorted into the row *Universal*. The columns represent the visualization methods, e.g., *Glyphs*, *Textures*, and *Line-based methods*, or concepts, like *Attribute space* methods or *Hybrid* methods, combining multiple basic visualization methods. The *Introduction to* column includes fundamental works, not necessarily including visualization. The table emphasizes where the recent research focus was and which areas could be interesting to explore in the future.

The references' color emphasizes if the corresponding paper has been published inside a visualization related conference or journal (red), or if it was published in an application-specific journal or conference (green). To give a complete overview, we added the papers discussed in the survey by Kratz et al. [KASH13] (blue).

3. Fundamentals

3.1. Tensor algebra

Mathematical concepts play a key role in data visualization. Hotz et al. [HBGW20] summarized mathematical concepts of the visualization literature and provided a taxonomy, especially for visualization beginners. However, not only the underlying mathematics but also the application-specific meaning of the data is essential when designing a useful (tensor) visualization. Both aspects will be covered in this section. Note that some operations introduced in this section are only defined for tensors of order two.

3.1.1. *Tensor definition*

The definition of a tensor also includes the specification of the underlying space. Therefore, let V be a real vector space. The dual space V^* is given by the set of all linear maps $\phi : V \to \mathbb{R}$. The elements of the vector space V are called contravariant, these of the dual space V^* covariant. An element of the set

$$\underbrace{V \otimes \cdots \otimes V}_{r\text{-times}} \otimes \underbrace{V^* \otimes \cdots \otimes V^*}_{s\text{-times}} \tag{1}$$

is defined as a tensor. Thereby, $V_1 \otimes V_2$ is the tensor product of the vector spaces V_1 and V_2. The number $q = r + s$ is called order of the tensors. The dimension n of a tensor is given by the dimension of the vector space V. The algebra of tensors of the vector space Equation (1) together with the tensor product as multiplication is called tensor algebra.

We use bold lower characters, like $\mathbf{a}$, $\mathbf{b}$, and $\mathbf{c}$, to describe tensors of order one, bold upper characters, like $\mathbf{A}$, $\mathbf{B}$, and $\mathbf{C}$, to describe tensors of order two, bold upper curved letters, like $\boldsymbol{\mathcal{A}}$, $\boldsymbol{\mathcal{B}}$, and $\boldsymbol{\mathcal{C}}$, to describe tensors of order three, upper curved font, like $\mathcal{A}$, $\mathcal{B}$, and $\mathcal{C}$, to describe tensors of order four, and double upper line letters, like $\mathbb{A}$, $\mathbb{B}$, and $\mathbb{C}$, for general tensors.

In most cases, an orthonormal basis is assumed, so there will be no distinction between co- and contravariant tensors. A tensor can also be defined as a multilinear map $\mathbb{T}$ of the q n-dimensional vectors $\mathbf{v}$ to the real numbers

$$\mathbb{T} : (\mathcal{V}^n)^q \to \mathbb{R}. \tag{2}$$

A tensor of order zero can be represented as a scalar, a tensor of order one as a vector, a tensor of order two as a matrix, and a higher-order tensor as an array of q dimensions.

A tensor field is a mapping that assigns a tensor to each position in a domain.

3.1.2. *General definitions*

An often used tensor operation is the tensor product or outer product of a qth-order tensor $\mathbb{A}$ and a rth-order tensor $\mathbb{B}$. It results in the $(q+r)$th-order tensor $\mathbb{C}$ as follows

$$\mathbb{C}_{i_1\dots i_q j_1\dots j_r} = \mathbb{A}\otimes\mathbb{B} = \mathbb{A}\mathbb{B} = A_{i_1\dots i_q}B_{j_1\dots j_r}. \tag{3}$$

The notation $A_{i_1\dots i_q}B_{j_1\dots j_r}$ is called Einstein notation. Thereby, the tensor is characterized by its coefficients. Another tensor operation is the tensor contraction. There is, for example, the single contraction

$$C_{i_1 i_2\dots i_{q-1} j_2\dots j_r} = \mathbb{A}\cdot\mathbb{B} = \sum_{k=1}^{n} A_{i_1\dots i_{q-1}k}B_{kj_2\dots j_r} \tag{4}$$

or the double contraction

$$C_{i_1 i_2\dots i_{q-2} j_3\dots j_r} = \mathbb{A}:\mathbb{B} = \sum_{k=1}^{n}\sum_{l=1}^{n} A_{i_1 i_2\dots i_{q-2}kl}B_{klj_3\dots j_r}. \tag{5}$$

A tensor contraction is characterized by the number of indices that are summed.

To simplify the notation, the Einstein summation convention is used in many cases. The contraction of two tensors is simplified by representing it without the sigma sign. Two tensors, represented by a single coefficient, are summarized about the coefficients that appear in both index sets

$$\sum_{k=1}^{n}\sum_{l=1}^{n} A_{i_1 i_2\dots i_{q-2}kl}B_{klj_3\dots j_r} = A_{i_1 i_2\dots i_{q-2}kl}B_{klj_3\dots j_r}. \tag{6}$$

An important value is the trace of a tensor. For a general qth-order n-dimensional tensor there exists more than one trace. Some literature uses the trace as the summation about the first and second index

$$\mathrm{tr}\,(\mathbb{T}) = \mathrm{tr}_{1,2}(\mathbb{T}) = T_{ssi_3\dots i_q}. \tag{7}$$

The definition of a totally symmetric tensor $\mathbb{T}$ with index set A is given by

$$\mathbb{T}_A = \mathbb{T}_{\pi(A)} \tag{8}$$

where $\pi(\cdot)$ describes the permutation of a set. The totally symmetric part of a qth-order tensor $\mathbb{T}$ is defined by

$$s(\mathbb{T}) = \frac{1}{q!}\sum_{\pi(A)} \mathbb{T}_{\pi(A)}. \tag{9}$$

Then, the asymmetric part $\mathbf{a}(\mathbb{T})$ can be defined by

$$a(\mathbb{T}) = \mathbb{T} - s(\mathbb{T}). \tag{10}$$

Based on these definitions, Backus [Bac70] defined a deviator as a traceless, totally symmetric tensor. Next to the total symmetry, there are other types of symmetry. A fourth-order tensor $\mathcal{T}$, for example, can have the major symmetry

$$T_{ijkl} = T_{klij} \tag{11}$$

or the minor symmetry

$$T_{ijkl} = T_{jikl} = T_{ijlk}. \tag{12}$$

There are other types of symmetry, but these are the important ones for this survey.

Many tensor definitions are only defined for tensors of order two. One way to generalize them for tensors of higher-order is to map the tensor onto one of order two. A fourth-order three-dimensional tensor with minor symmetries has 21 independent components. Thus, it can be represented in a 6×6 matrix. One such mapping is given by the so-called Voigt mapping

$$\mathbf{C}^V = \begin{pmatrix} C_{1111} & C_{1122} & C_{1133} & C_{1123} & C_{1113} & C_{1112}\\ C_{2211} & C_{2222} & C_{2233} & C_{2223} & C_{2213} & C_{2212}\\ C_{3311} & C_{3322} & C_{3333} & C_{3323} & C_{3313} & C_{3312}\\ C_{2311} & C_{2322} & C_{2333} & C_{2323} & C_{2313} & C_{2312}\\ C_{1311} & C_{1322} & C_{1333} & C_{1323} & C_{1313} & C_{1312}\\ C_{1211} & C_{1222} & C_{1233} & C_{1223} & C_{1213} & C_{1212} \end{pmatrix}. \tag{13}$$

The matrix (13) has the advantage that it directly contains the coefficients of the original tensor. However, it does not preserve the tensor norm and is, therefore, no tensor itself. Another mapping is more common in the theoretical mechanics' community and is called the Kelvin mapping or Mandel notation. It preserves tensor properties by transforming the fourth-order three-dimensional tensor with minor symmetries into a second-order six-dimensional tensor with the following coordinate matrix

$$\mathbf{C}^K = \begin{pmatrix} C_{1111} & C_{1122} & C_{1133} & \sqrt{2}C_{1123} & \sqrt{2}C_{1113} & \sqrt{2}C_{1112}\\ C_{2211} & C_{2222} & C_{2233} & \sqrt{2}C_{2223} & \sqrt{2}C_{2213} & \sqrt{2}C_{2212}\\ C_{3311} & C_{3322} & C_{3333} & \sqrt{2}C_{3323} & \sqrt{2}C_{3313} & \sqrt{2}C_{3312}\\ \sqrt{2}C_{2311} & \sqrt{2}C_{2322} & \sqrt{2}C_{2333} & 2C_{2323} & 2C_{2313} & 2C_{2312}\\ \sqrt{2}C_{1311} & \sqrt{2}C_{1322} & \sqrt{2}C_{1333} & 2C_{1323} & 2C_{1313} & 2C_{1312}\\ \sqrt{2}C_{1211} & \sqrt{2}C_{1222} & \sqrt{2}C_{1233} & 2C_{1223} & 2C_{1213} & 2C_{1212} \end{pmatrix}. \tag{14}$$

3.1.3. *Second-order tensor definitions*

The mostly used tensors are second-order three-dimensional tensors $\mathbf{T}$. For which we note some common definitions.

An interesting value is the so-called tensor norm which is given by a transformation that maps the tensor to a scalar. The second-order tensor norm is given by

$$|\mathbf{T}| = \sqrt{\mathbf{T}:\mathbf{T}}. \tag{15}$$

To describe a symmetric tensor, the so-called invariant space can be used. An invariant is a scalar function

$$\beta : Sym(\mathbb{R}^3\otimes\mathbb{R}^3)\to\mathbb{R} \tag{16}$$

that is invariant to the operations of rotation of $\mathbb{R}^3$. The invariant space, i.e., the space of all invariants, of a second-order symmetric three-dimensional tensor is three-dimensional and is spanned, e.g., by the three eigenvalues.

3.2. Tensor decomposition

One of the big challenges in tensor visualization is the multitude of values and the variety of information that can be derived from a

tensor. In general, not all this information can be visualized at once. One way to approach this challenge is to decompose the tensor into independent parts and analyze them separately. For example, the analysis of a vector field and a symmetric, second-order tensor is easier than the visualization of a second-order asymmetric tensor.

Different tensor decomposition methods can be used. A common method is to decompose a tensor $\mathbb{T}$ of arbitrary-order in its totally symmetric and its asymmetric part

$$\mathbb{T} = \mathbb{S} + \mathbb{A}, \tag{17}$$

where $\mathbb{S}$ is the totally symmetric part Equation (9) and $\mathbb{A}$ the asymmetric part Equation (10) of $\mathbb{T}$.

3.2.1. *Second-order tensor decomposition*

Many of the tensor decomposition methods are only defined for second-order tensors because they are the most often analyzed ones. Hence, let $\mathbf{T}$ be a second-order tensor.

The polar decomposition is one example of a tensor decomposition. Therefore, $\mathbf{T}$ is split into the pure rotation $\mathbf{Q}$ and the pure stretch $\mathbf{S}$

$$\mathbf{T} = \mathbf{Q} \cdot \mathbf{S}. \tag{18}$$

The spectral decomposition is another example. Thereby, the symmetric n-dimensional tensor $\mathbf{T}$ will be represented by its eigenvectors γ_i and eigenvalues λ_i

$$\mathbf{T} = \mathbf{\Gamma}\mathbf{\Lambda}\mathbf{\Gamma}^T = \sum_{i=1}^{n} \lambda_i \gamma_i \gamma_i^T, \tag{19}$$

with $\mathbf{\Lambda} = \mathrm{diag}(\lambda_1, \ldots, \lambda_n)$ and $\mathbf{\Gamma} = (\boldsymbol{\gamma}_1, \ldots, \boldsymbol{\gamma}_n)$.

3.2.2. *Fourth-order tensor decomposition*

Next to the second-order tensor decompositions, there are also methods to decompose other tensors, like fourth-order tensors. To compute a polar decomposition of a three-dimensional fourth-order tensor with major- and minor symmetries, Neeman et al. [NBJ*08] used the Kelvin mapping (see Equation (14)) and performed a polar decomposition on the resulting tensor of order two in six dimensions.

The spectral decomposition of a fourth-order n-dimensional tensor $\mathcal{T}$ with major- and minor symmetries is given by

$$\mathcal{T} = \sum_{i=1}^{n} \lambda_i \mathbf{M}_i \otimes \mathbf{M}_i, \tag{20}$$

where λ_i are the eigenvalues and $\mathbf{M}_i$ the second-order eigentensors of $\mathcal{T}$.

The deviatoric decomposition of the fourth-order tensor with minor and major symmetries is given by Zou et al. [ZTL13] (see also Hergl et al. [HNS20])

$$\mathcal{C} = \mathcal{D} + 6\mathbf{s}(\mathbf{ID}) + 3\mathbf{s}(\mathbf{II}d) + \varphi(\hat{\mathbf{D}}) + \frac{1}{2}\varphi(\mathbf{I}\hat{d}), \tag{21}$$

where $\mathcal{D}$, $\mathbf{D}$, $\hat{\mathbf{D}}$, d and $\hat{d}$ are deviators, $\mathbf{s}(\cdot)$ describes the symmetrization, and φ is an isomorphism between symmetric second-order tensors and asymmetric fourth-order tensors.

3.3. Tensors in structural mechanics, bio-, and geomechanics

Physical phenomena in engineered structures, biological tissues, and the geosphere are commonly described by physical fields using the methods of continuum physics [Wri08, Dog00, Hol00]. The principal constituents of such theories are largely identical between these fields of observation:

- *Differential geometry* is used to describe geometric aspects of the problem, such as changing positions of particles themselves or the relative changes of positions between neighboring particles. This leads to vector-valued quantities, like displacements and velocities describing positional changes, as well as tensor-valued quantities such as deformation gradients, strain tensors, etc. describing rotations and deformations.
- *Balance relations* are established for conservation quantities such as mass, linear and angular momentum, energy, charge, etc., which are scalar and vector-valued quantities. The action of vector-valued quantities along oriented area elements again leads to the introduction of second-order tensors, such as stress tensors , which describe the mechanical loads the material is subjected to.
- Because the number of equations provided by differential geometry and the balance relations is not sufficient to solve for all unknowns, certain quantities need to be linked by *constitutive relations*. In contrast to the former two aspects generally considered to be universally valid, the constitutive relations describe material- and problem-specific features. An example is the heat conductivity, linking temperature gradients and heat fluxes. As both are vector-valued, the linear mapping between the two is generally a second-order tensor. Similarly, to describe the relationship between the amount of deformation a material undergoes and the resulting mechanical forces inside the material, the stiffness tensor linearly maps a strain increment into a stress increment and can thus be recognized as a fourth-order tensor.

It can be seen that in all application areas, similar tensorial quantities or physical objects appear. Of course, the specific constitutive relations will differ between disciplines because the human heart muscle responds to mechanical loading in a different manner than a porous sandstone layer several kilometers below the earth's surface. However, in both cases measurements or numerical simulations generate tensors describing stress, strain, or material properties, which need to be visualized.

Similar statements can be made when distributions of certain properties need to be described: whether the bedding plane of sedimentary rock, the collagen fiber-reinforcement of a tendon, or a technical fiber-reinforced composite material are of interest — in all cases, objects such as fourth-order stiffness tensors or second-order structure tensors can be used to describe material anisotropy.

Consequently, scientific visualization faces similar challenges in structural mechanics as it does in bio- or geomechanics.

4. Tensor Visualizations

Visualizations are probably the fastest way to understand the huge amount of information encoded by tensors. In the following sections, recent tensor visualization methods are presented and categorized according to their type, if they are glyphs (see Section 5), geometry-based (see Section 6), texture-based (see Section 7), of topological nature (see Section 8), or if they show multivariate data (see Section 9).

5. Tensor Glyphs

Glyphs are probably the most common way to visualize tensors across all discussed application areas. They are used to visualize single tensors in selected positions as well as the combination of different tensors. In many cases, they are combined with other visualization methods.

Glyphs are geometrical objects that depict information of the data by geometric or optical properties, like shape, size, color, transparency, or texture. Glyph visualization is a local method to describe data. In accordance with Kratz et al. [KAH14] the questions 'Which information to chose?' and 'How to map the information onto geometry?' are important for glyph design. The glyphs can be used, for example, for debugging, to evaluate data quality, to visualize an overview, or to probe for single data points. They also promote the idea that relevant tensor invariants should play a role when designing an application-specific glyph. Generally, a glyph should be easy to understand and faithfully represent the information included in the data. This is no trivial task because data can contain much information. The following specifications of Schultz and Kindlmann [SK10] can be used as guidance during the tensor glyph design process:

- Preservation of symmetry,
- Continuity,
- Disambiguity, and
- Invariance under scaling and eigenplane projection.

Furthermore, the placement is significant for the perception of information from a glyph. Ward [War02] described two differentiating placement strategies: On the one hand, the 'data-driven glyph placement' means using the data to specify or compute location parameters. He further subdivides this strategy into a *raw data* and *derived data* strategy. The other strategy called 'structure-driven glyph placement' makes assumptions about a relationship between data points. In context with tensor field visualization, several methods for dense glyph placement strategies have been introduced [KW06, FHHJ08, KASH13].

The visualization method is used to structure the latter visualization method chapter. But there is no unique classification of the different glyph design to specific used visualization methods. Through the huge number of glyph designs, no classification would make it difficult to get an overview about the designs. Glyphs are specific to the application, and the tensor type, therefore, not always transferable. Hence, this section is structured by tensor types. Following this, the applicableness of different glyph designs for specific applications could be worth to evaluate in a separate work.

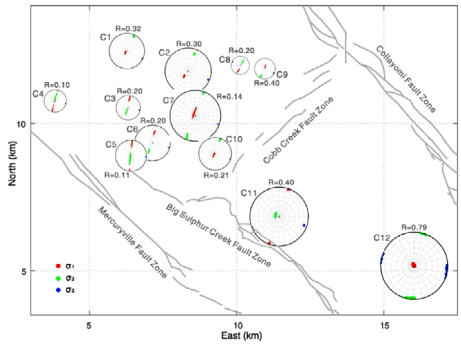

Figure 4: *Visualization of the principal directions of stress tensors using stereographic projections (image from [YVAB18]).*

5.1. Stress (and Strain) tensors

Stress and the mathematically equal strain tensor are frequently visualized using glyphs in all applications. Thereby, the most common type is the ellipse in two and the ellipsoid in three dimensions, even though they have strong limitations, including perceptional issues, and they fail to distinguish positive and negative stresses. Variants dealing with these issues have been developed, e.g., superquadric glyphs [SK10]. They are generally applicable to all symmetric second-order tensors. Patel and Laidlaw [PL20] evaluated some glyph-based visualizations for stress tensors, including the original superquadric glyphs and a new colored version specifically designed for stress tensors to enhance the perception of the principal directions. More variants of stress tensor glyphs, including Haber glyphs, Reynolds glyphs, HWY glyphs, quadric surfaces, plane-in-a-box glyphs, and the superquadric glyphs are summarized in the survey by Kratz et al. [KASH13].

In structural mechanics, simulations typically generate dense stress and strain fields. Stress visualizations are used for analyzing the simulation results but also for the analysis of the simulation process itself. E.g., to evaluate different time-stepping schemes, Mohr et al. [MBH*08] identified regions exhibiting large variances to display the intrinsic qualities of the data and the algorithm's numerical behavior. The comparison overlays ellipsoidal glyphs differentiating between negative and positive stress.

The stress tensor in geomechanics is typically extracted by moment tensor inversion and is visualized by plotting its principal stresses on a disk with a stereographic (lower hemisphere) projection [Vav14]. For example, Boyd [Boy18] and Yu et al. [YVAB18] used inversion and visualization for geothermal reservoirs (see Figure 4). Most visualization techniques are derived from moment tensor analysis, which are described in an own Section 5.3.

In biomechanics, glyphs are also used for the representation of stresses and strains. Selskog et al. [SBWK01] visualized the myocardial strain-rate tensors derived from phase-contrast MRI using ellipsoidal glyphs. For the visualization of the residual stress tensor in soft tissues and deformations due to cutting, Wu et al. [WBWD12] defined a two-dimensional glyph. It is displayed on the skin of the human body to illustrate the effect of small round incisions. The glyph encodes the major principal direction, expected

tissue behavior, and the magnitude of the residual stress component in the direction of the cutting surface normal.

5.2. Stress gradients

Not only stresses but also its changes are relevant when analyzing material performance. It can influence the stability limit of a technical component, as pointed out by Zobel et al. [ZSS17]. They introduced visualizations of tensor gradients including the stress gradient. The gradient was visualized by two super-positioned distinct-colored ellipsoids, one indicating the average change of all stress vectors and the other showing an actual stress tensor. They also included a second approach utilizing the envelope of Reynolds glyphs encoding the eigenvalue sign by color.

5.3. Moment tensor

In geomechanics, one single moment tensor describes a single seismic (or acoustic) event resulting in sparse but multifaceted data. Hence, they are predestined for a visualization using glyphs. Often the glyphs are designed to jointly visualize many aspects of these seismic events, which mark them as highly advanced. The tensor itself and its glyphs are not well known to the visualization community. Almost all moment tensor visualization methods have been published in the geomechanical community. We summarize some of these glyphs common in geomechanics in the following because they show an interesting way of visualizing data.

Le Gonedic et al. [LGSWN14] introduced the simplest glyph to visualize the moment tensor. Their glyph is a sphere shown in a three-dimensional space and colored according to the type of the seismic event at its location. Neeman [Nee04] introduced a glyph to visualize components of the moment tensor simulating an oil flow. It is a small plane oriented along the fracture plane spanned by the two dominant eigenvectors and scaled by the magnitude of the shear stresses. Baig et al. [BUM*12] visualized the fracture planes of the moment tensor, which marks the orientation of gaps inside the rock. They used so-called *penny-shaped glyphs*, which are circles used to visualize the orientation of the fracture planes. Color encodes the type of seismic events as opening or closing of a fracture or shear event. A more complex glyph by Cladouhos et al. [CUS*15] displays microseismic events during the stimulation of a fracture network. It connects arrows, indicating maximal and minimal principal stresses, and a sphere, indicating volume gain or loss. Another example is the glyph by Leaney et al. [LYC*14], where a wireframe of a sphere is used for the volume change and two shifted cylinders for the orientation of the fracture plane. Cylinders' thickness describes the opening or closing of the fracture. Using these components, more information, like the opening angle or the amount of shearing, can be visualized. Chapman and Leaney [CL12] introduced a glyph based on a new moment-tensor decomposition for seismic events in anisotropic media. A sphere represents the volume change of a fracture and color distinguishes the sign related gains and losses. Like one of Saturn's rings, a disc represents the fracture plane. An arrow shows the displacement discontinuity, which describes the propagation of the fracture.

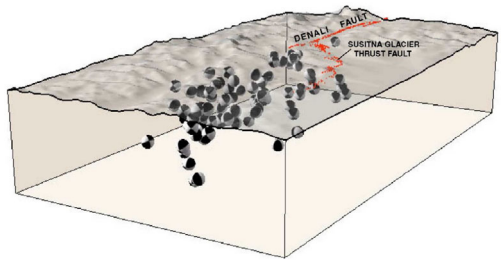

Figure 5: *Visualization of multiple seismic events during the Denali Fault earthquake in 2002 using beach ball glyphs (image from [LH07]).*

One of the most frequently used glyphs in geomechanical papers are beach balls [Cro04]. Beach balls are lower-hemisphere stereographic projections showing two black and two white quadrants (see Figure 5). The glyph encodes the directions of the three orthogonal pressure (P), tension (T), and null vectors (N) of a moment tensor. According to Cronin [Cro04] they allow for a fast interpretation of the represented moment tensors by scientists. Additional information can be encoded into the size and the color of a beach ball [Boy18, GD11, ZYZ*19, WGSC18, LH07, DP08]. They also have been extended by other geometric primitives, e.g., arrows to enhance the perception of pressure and tension vectors [UBG*12, UBGB10]. Additional ellipses emphasize the orientation of the fractures colored due to their opening or closing characteristic [LYC*14].

Willemann [Wil93] clustered moment tensors of different events, and visualized them as separate beach balls. Alvizuri et al. [ASKT18] used them in combination with the lune and rectangle plot of Tape and Tape [TT12, TT15] to visualize all characterizing properties of a seismic event.

Furthermore, moment tensor analysis and visualization are used to investigate the stress and the structure of rock as they also affect the orientation of the emerging cracks [FKGR03]. For example, Liu et al. [LLP*18] investigated the behavior of granite and sandstone under compression using moment tensor analysis. They used simple glyphs consisting of a small disc, which are oriented orthogonal to the normal of the fracture surface, and arrows visualizing the direction the fracture evolves in.

5.4. Orientation and alignment tensors

Another tensor often visualized by glyphs is the orientation tensor. The (fiber) orientation tensor describes the distribution and the frequency of bidirectional unit vectors per infinitesimal small area. It is relevant to describe microscopic anisotropic structures of the material. Zobel et al. [ZSS15] combined the stress and this fiber orientation tensor to construct a new glyph to indicate failure in a fiber-reinforced polymer component. Superquadrics visualize the fiber orientation tensor and color distinguishes non-critical, critical, and fatal regions. It was combined with a cone based on the stress, where the alignment of these objects provides failure indication for a given region.

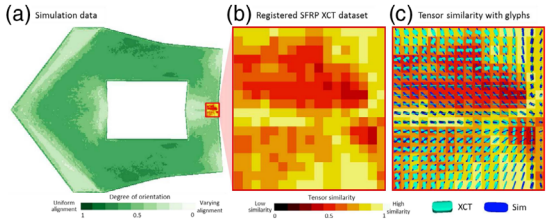

Figure 6: *Comparison of X-CT data with its simulation. a) showing the whole component domain and the zoomed-in area, with b) tensor similarity as heat map, and c) an overlay of superpositioned fiber orientation superquadric glyphs (image from [WAS*18]).*

Visualizing fiber orientation is also interesting for yhe reconstruction and processing, e.g., of X-CT images. Various frameworks to extract fibers and their orientation exist [WAL*14, BHA*15, BWW*17]. Weissenböck et al. [WAS*18] introduced an interactive framework for comparing X-CT data with other X-CT data or simulations of fiber-reinforced polymers. They calculated three similarity measures for the fiber orientation tensor: the degree of orientation, the angle between the main directions, and the component-wise tensor similarity. They are visualized as heat maps to show the correlations. Superpositioned superquadric glyphs are used for a detailed comparison (see Figure 6).

Another method to describe the symmetries of a material is by using Orientation Distribution Functions (ODF), which can also be tensors of higher-order. Moakher and Basser [MB15] presented ODFs of different orders and their related tensors in closed-form expressions for all ranks, especially for rank one to four. Besides the basic mathematics, ODFs of a specific anisotropy type, as well as axiallysymmetric ODFs, were discussed.

Arisen from the special case of Nematic Liquid Crystals (NLC), describing an intermediate phase between the liquid and solid phase of specific materials, a superellipsoid glyph design for their molecule alignment was presented [JKM06]. The, therefore, described NLC alignment tensor is similar to the fiber orientation tensor. This method can further be used for any real symmetric traceless tensor. Later, Jankun-Kelly et al. [JKLSI10] evaluated four different tensor glyphs: boxes, ellipsoids, cylinders, and superquadrics. They analyzed which of them are the best to encode tensorial variables of the NLC alignment tensor, like the orientation, uniaxiality, and biaxiality. In the end, they conducted that superquadrics are less error-prone than the other glyphs.

To assess the anisotropic structure of bio-materials, DTI is also used especially in context with the myocardium, the heart muscle. Thereby the diffusion tensor provides an approximation of the orientation distribution of the muscle fibers. Often ellipses or ellipsoids are overlaid over the imaging data [GDMS*15, LNY*18]. One also sees hedgehog-like visualizations plotting lines or vectors in the major eigenvector direction [GYLG20]. Ennis et al. [EKH*04] demonstrated the use of superquadric glyphs to visualize fiber orientation.

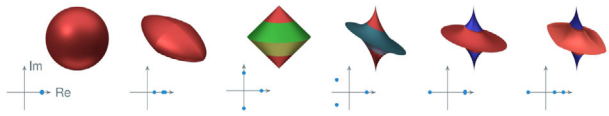

Figure 7: *Glyph design for general second-order tensor glyphs. These glyphs represent different tensors with their respective eigenvalues shown in their real and complex plane (image from [GRT17]).*

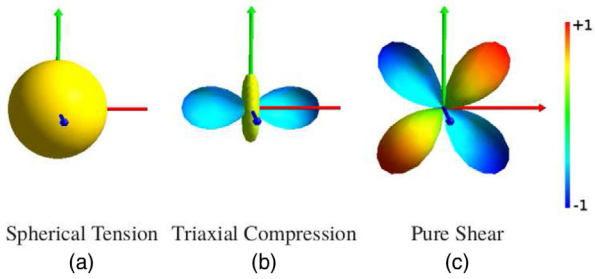

Figure 8: *Decomposing the stiffness tensor by a spectral decomposition allows visualizing the rotation part and the stretch part by Reynold's glyphs. The figure illustrates different stress modes (image from [NBJ*08]).*

© 2008 The Author(s)
Eurographics Proceedings © 2008 The Eurographics Association.

5.5. Asymmetric second-order tensors

Seltzer and Kindlmann [SK16] designed a new tensor glyph expanding the class of generic tensor glyphs to asymmetric second-order tensors in two dimensions. For the three-dimensional domain, Gerrits et al. [GRT17] presented a glyph design for general second-order tensors, which especially includes the visualization of two-dimensional tensors. It uses color coding, defining positive and negative eigenvalues, as well as counter- and clockwise swirling behavior in terms of imaginary parts of the eigenvalues. Additionally, the shape defines the signs of the real eigenvalue parts. A so-called *eigenstick* is used for vanishing eigenvalues, to display the related eigenvector. Figure 7 shows the glyph design for various sets of eigenvalues.

5.6. Stiffness tensors

The stiffness tensor is the most frequently visualized higherorder tensor. With all the symmetries described in Section 3.3, the stiffness tensor has 21 independent coefficients. As they depend on the local coordinate system, they are hard to interpret even for experienced engineers.

For visualization, the focus is at first on the tensor decomposition, to make the tensor more accessible. Neeman et al. [NBJ*08] transferred the polar decomposition to the stiffness tensor. The eigentensor to the minor eigenvalue of the resulting stretch part is visualized with a Reynold's glyph (see Figure 8). In their context, the smallest

eigenvalue describes the most fragile property and, therefore, the most important information. In contrast, Kriz et al. [KYHR05] analyzed the stiffness tensor by calculating the plane waves. They visualized the resulting shapes by deforming a sphere by these waves.

Although it is not the focus of the engineering community to visualize the stiffness tensor when analyzing, there exist some basic visualizations. Helbig [Hel15] analyzed the stiffness tensor by performing a spectral decomposition using the Kelvin mapping. Each eigenstrain is represented as a cube. Therefore, the eigenvectors of the eigenstrain define the coordinate system. Arrows on the faces of the cube, scaled by the eigenvalues of the eigenstrain, represent compression. Böhlke and Brüggemann [BB01] described a generalization of the Bulk- and Young's modulus depicted in two ways: A stereographic projection onto a sphere surface and a glyph enveloping every direction, given by the Young's modulus in the considered direction. An application of this glyph is given by Böhlke and Lobos [BL14]. The consequence for the elasticity modulus is represented in a glyph describing the modulus in each direction at one point. Jianping et al. [JFK*15] simulate anisotropic materials by assuming the anisotropy type and the local coordinate system. With the deformation gradient, the new alignment is computed by deforming the normals of the symmetry planes of the assumed material. The method is tested by representing the deformation with the help of line segments. Backus [Bac70] gave a derivation of the deviatoric decomposition and represented the deviators of the stiffness tensor by five multipole set presentations (one set of normalized vectors for each deviator). Based on the deviatoric decomposition, Zou et al. [ZTL13] calculated a characteristic function. It equals zero if the normal in this place is a mirror plane normal. This mapping is represented on the unit disk to identify the anisotropy types. Also, based on the deviatoric decomposition, Hergl et al. [HNKS19] designed a glyph to present the anisotropy types and the symmetries of the described material. The symmetries of the deviators describe the symmetries of the stiffness tensor and give information about the anisotropy type of the described material. The base of the glyph is a set of tubes representing the symmetry plane normals. A sphere in the center of the tubes gives information about the anisotropy rate.

5.7. Uncertainty tensors

Whenever ensembles of tensor fields are analyzed, uncertainty becomes an important aspect and increases the complexity even further. Abbasloo et al. [AWHS15] proposed one of the first frameworks dealing with the uncertainty of symmetric second-order tensors. They provide different levels of detail for the visualization of tensor covariance. Next to an overview of the variance, details about specific variabilities, like shape and orientation, are shown. The principal modes were translated into six eigentensors with respective eigenvalues. The two most extreme cases of each eigenmode were displayed using superquadric glyphs of complementary color. In the context with Diffusion MRI, Schultz et al. [SSSSW13] developed a new glyph (called HiFiVE) to illustrate the uncertainty in fiber orientations. It is based on the estimation and decomposition of the fiber distribution into the main direction and a non-negative residual. The most recent work by Gerrits et al. [GRT19] visualized the uncertainty tensor as a set of mean and covariance tensors. They used standard glyph designs for the mean tensor (see Figure 9) and a translucent hull to encode the uncertainty as a surface with an offset by its directional magnitude. The glyphs help to find differing regions for all processed fields, where the assumption of a Gaussian normal distribution holds [KGG*20].

Figure 9: *Uncertainty glyph using superquadric (left) and the glyph from Gerrits et al. [GRT17] (right) as base for an indefinite mean tensor (image from [GRT19]).*

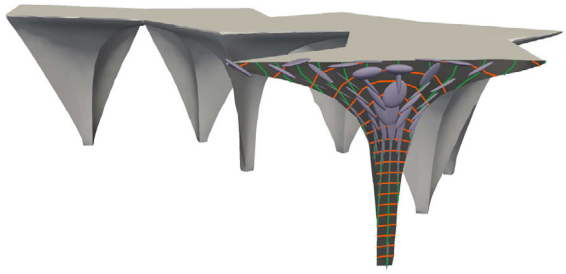

Figure 10: *Stress alignment inside a pavilion as a basis for load optimized Michell Trusses (image from [AJL*19]).*

6. Geometry-based Methods for Tensor Fields

Local methods, such as glyphs, provide detailed information about single tensors. However, local methods quickly suffer from cognitive overload, visual clutter, and occlusion. Besides that, they fail to provide a more continuous view of the structure of a tensor field. Geometry-based methods are used to encode more global information about field attributes.

Tensor lines – Dickinson [Dic89] introduced tensor lines, also known as principal stress lines or fiber tracks. They follow eigenvector directions and are a generalization of streamlines to second-order tensor fields. For each eigenvector field, there is one family of tensor lines. Since eigenvectors do not point in a direction, the terms forward and backward do not have a semantic meaning. Therefore, they are usually integrated back and forth from the seed point.

In structural mechanics, stress tensor lines can represent major load paths and have been used to guide geometry optimization of mechanical components [KSZ*14, SKZ*15, WAWS17, KLC16]. Volumetric Michell Trusses, structures following the maximum strain, have been designed using a similar concept [AJL*19]. Simple glyphs and stress tensor lines are used for their representation (see Figure 10).

Tensor lines are also applied in biomechanical applications. In context with the orientation distribution or diffusion tensors, they are interpreted as major fiber or structure direction of the material. Especially in the context of visualizing the tissue of the myocardium, they are used to visualize the muscle fiber structure [GDMS*15, LNY*18, DSB*19]. Wu et al. [WBWD12] presented

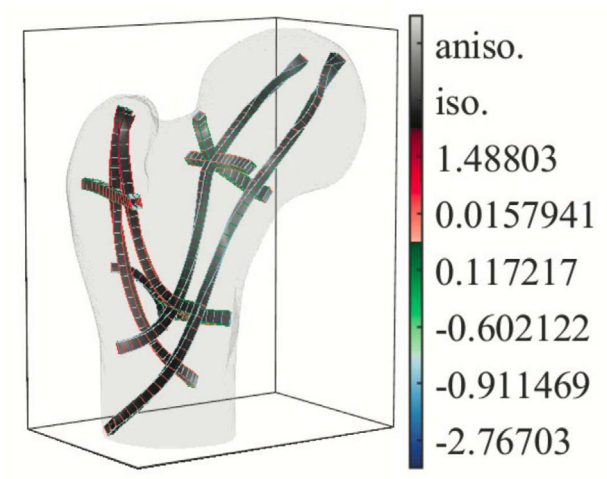

Figure 11: *Beams are used to visualize the stresses in a three-dimensional femur (image from [WWW20]).*

an interactive method to compute and visualize patient-specific residual stress in soft tissues, which is, among others, visualized using tensor lines.

Hyperstreamlines – Hyperstreamlines [DH92, DH93] are an extension of tensor lines. Either elliptical or cross-shaped tubes are used instead of lines. The major eigenvector again gives the tube's direction. Its elliptical cross-section or cross-shape is defined by the intermediate and minor eigenvectors. Sometimes also, color is used to encode a selected eigenvalue.

Tensor Spines – As a modification of hyperstreamlines, Kretzschmar et al. [KGSS20] introduced tensor spines. Instead of elliptical cross-sections, a circular tube and two perpendicular surfaces are combined. They are based on the relation between the traced eigenvalue-eigenvector pair and the remaining pairs. They suit especially indefinite symmetric second-order tensor fields and help identifying points where the maximum of absolute eigenvalues swaps between major and minor.

Stress nets – Stress nets give a sparse overview of the stress/shear directions in a given two-dimensional field [WB05]. An approximately uniform grid is deformed and aligned according to the stress/shear directions. The sparsity of the method leaves space for the visualization of additional attributes, e.g., using color according to a derived scalar field, such as the eigenvalues or other invariants.

Globally conforming lattice – Wang et al. [WWW20] introduced a globally conforming lattice for two- and three-dimensional stress tensor fields. They used beam elements that follow the principal stresses, as depicted in Figure 11. Additionally, color encodes the magnitude of compression or tension. The size of the beam elements is scaled according to anisotropy.

Hyperstreamsurfaces – Jeremić et al. [JSF*02] introduced another extension to hyperstreamlines, the hyperstreamsurfaces. They used a set of points on open (or closed) curves to construct a set of tensor lines, which are then connected using polygons to form the hyperstreamsurfaces.

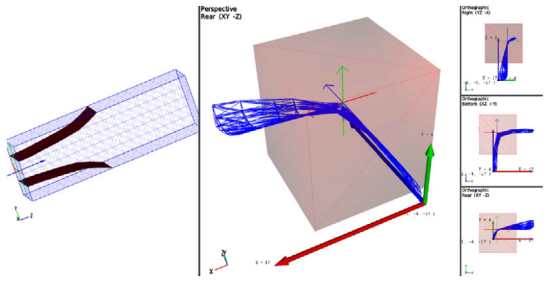

Figure 12: *The intersection of the interactor (red shaded box, right and middle panel) and the mesh, which is transferred from the domain (left) to the invariant space (mid and right), defines the fiber surface, rendered in the domain (image from [RBN*19]).*

Deformed geometry – To understand general, second-order tensor fields, Boring and Pang [BP98] presented a deformation-based technique to visualize the impact of a field on planar surfaces. The method has also been extended to volume objects, like spheres or grids, using volume deformation methods. [ZP02].

Fiber Surfaces – Fiber surfaces are an extension of isosurfaces to a two- [CGT*15], three- [RBN*19], or n-dimensional codomain [BRP*20]. Like isosurfaces, they show regions inside the domain where specific isovalues appear, however, considering combinations of isovalues from the different attributes in the codomain that are visualized simultaneously (see Figure 12). They share the property of separating the domain if they split the range.

7. Texture-based Methods for Tensor Fields

Another approach are texture-based methods, giving an overview of a tensor field on slices, surfaces, or in a few examples also in three dimensions. Most of the methods in this area are based on the classical Line Integral Convolution (LIC) method for vector fields, which has been extended to tensor fields. Furthermore, they are typically combined with geometry-based methods.

HyperLIC – HyperLIC generates a texture by filtering a noise texture using a two-dimensional convolution filter [ZP03a]. The filter is a geometric primitive defined by the tensor placed over each location and blurs the texture using all eigenvector fields. The filter does not take the sign of the eigenvalue into account and thus is especially suitable for positive definite tensors. Therefore, HyperLIC highlights the anisotropic properties in a tensor field.

Fabric-like visualization, tensor LIC – Fabriclike visualization of tensor field data on arbitrary surfaces [HFH*04, HFH*06] focuses on the two principal directions of the tensor projected onto the surface. The free parameters of the noise texture are used to encode the scalar invariants of the tensor. An image-space variant[EHHS12] supports a fast computation of the texture. The method has been applied in multiple application contexts, including the visualization of stresses for the geomechanical simulation of subduction zones [HFH*05].

Tensor LIC combination with brushing and linking – Kratz et al. [KSZ*14] proposed an approach by visualizing principal

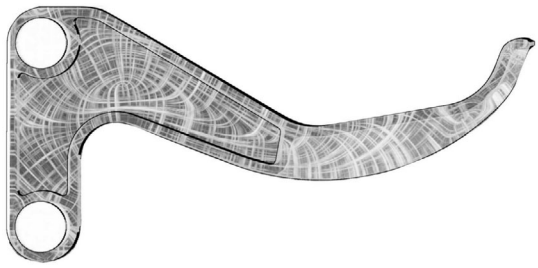

Figure 13: *LIC on a lever brake, giving engineers a visual guide for possible stress aligned stiffener (image from [KSZ*14]).*

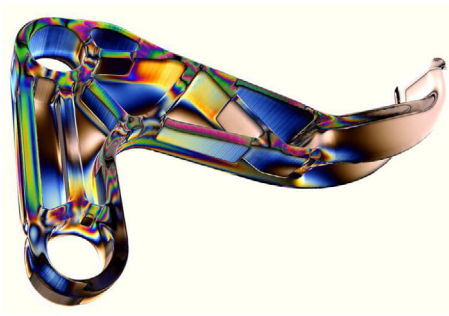

Figure 14: *Photoelasticity raycasting applied to a lever brake, simulating a polariscope analysis (image from [BES15]).*

stresses on a cutting plane. Their tool came with a brushing and linking framework combined with LIC to show force paths (see Figure 13). Based on them, the engineers brought internal ribs into the previously defined design space. The small changes improved the overall stiffness and durability by a lower material use.

LIC combination with streamsurfaces – Song et al. [SLZZ15] presented a comprehensive method for encoding all three eigenvector fields of stress and strain tensor fields by combining LIC and streamsurfaces. They used sparse noise imaging instead of white noise to support effective visualization.

Tensor lines with isocontours – In order to facilitate the usage of tensor lines for engineers, Moldenhauer [Mol18] presented a programming-free approach for the calculation of tensor lines on surfaces. Therefore, he used the thermal conduction analysis by setting the principal heat conductor directions to the eigenvectors of a tensor field. The results of the analysis are different isocontours indicating tensor lines.

Textures from anisotropic Voronoi tessellations – Kratz et al. [KASH13] proposed textures generated from anisotropic Voronoi tessellations of boundary surfaces. The orientation and shape of the Voronoi cells are determined by a tensor field given on a surface. Textures, e.g., have been applied to imitate the structure of endothelial cells of a blood vessel based on the wall shear stress resulting from the blood flow. A texture resembling this is mapped into the anisotropic Voronoi cells.

Textures from topology – Two-dimensional tensor field topology generates a segmentation of the domain in regions of similar tensor behavior, whose properties are encoded by texture parameters [ASKH12]. This approach supports the generation of a large variety of textures, e.g., stripe patterns, fabric, knitting, or basketwork patterns.

Photon distribution – Zheng and Pang [ZP03b] presented an approach utilizing parallel light rays that were deformed by the tensor field. This method can produce results similar to hyperstreamlines [DH93]. In addition, they presented the so-called photon distribution. Here, a prism that produces different rays of different wavelengths out of a single ray is used. Lastly, they introduced the lens simulation, which uses a given image and shows the projected and deformed images from different viewpoints.

Bußler et al. [BES15] presented a similar approach for real-world polariscope analysis to further extend the correlation of tensor fields and light. They integrated the photoelasticity into a raycasting algorithm, in order that the tensor field refracts incoming light. Photoelasticity is based on the stress-optic law and provides the possibility of showing the stress distribution, especially around material discontinuities. While real-world experiments are limited to transparent materials, the proposed visualization method can provide the stress distribution inside arbitrary domains by assuming a translucent hull (see Figure 14).

Three-dimensional textures – In context with the visualization of the strain-rate tensors from the human heart muscle obtained from Phase Contrast Magnetic Resonance Imaging (PC-MRI), Sigfridsson et al. [SEHW02] proposed a volumetric texture visualization. The texture results from a noise field by applying adaptive high-pass filtering in direction with minor eigenvalues (similar to LIC). Thereby, the filters do not respect the sign of the eigenvalues. Zhang et al. [ZDL*11] synthesized solid textures using two-dimensional exemplars that locally agree with a tensor field derived from user sketched curves.

8. Topological Tensor Field Analysis

According to Heine et al. [HLH*16], topology-based visualizations can be summarized as follows:

> *'Topology-based visualization uses topological concepts to describe, reduce, or organize data in order to be used in visualization. Typical topological concepts are, e.g., topological space, cell complex, homotopy equivalence, homology, connectedness, quotient space. Typical visualization uses are, e.g., to highlight data subsets, to provide a structural overview, or to guide interactive exploration.'*

Central elements of topological analysis for the two-dimensional case are degenerate points (alias critical points) and separatrices dividing areas of different behavior. As most topological concepts, tensor field topology provides a global field analysis.

The theory was originally developed by Delmarcelle and Hesselink [DH94] for symmetric second-order tensor fields of dimension two and later dimension three by Hesselink et al. [HLL97]. Therefore, they mainly generalize the concepts from vector field topology. Until now, this is still the only setting where a more or

less complete theory exists. Since then, much effort was applied to extend the scope to higher-orders and the two-dimensional asymmetric case. Despite the significant advances over the last years, there are still many fundamental questions open, and the use of these methods in real-world applications is still in its infancy. Additionally, there is almost no work on higher-order tensor topology. However, Schultz [Sch11] presented some first steps towards a generalization.

8.1. Two-dimensional symmetric second-order tensor fields

In the two-dimensional symmetric case, topology defines a segmentation of the domain in regions of uniform tensor line behavior. The segmentation is given by a topological skeleton built from degenerate points and separatrices, connecting these points [DH94]. Degenerate points are points where both eigenvalues are the same. Besides the detection of degenerate points, the question of the features' interpretation is an often mentioned problem. Zhang et al. [ZGZ17] showed the first approaches to analyze the tensor topology in an engineering application. In their work, they applied some simulations to find a correlation between tensor properties of the stress tensor and the degenerate points. Gao [Gao18] made similar calculations and came to similar results.

8.2. Three-dimensional symmetric second-order tensor fields

In the three-dimensional symmetric case, different types of degenerate features, defined by the multiplicity of the eigenvalues, exist. If two eigenvalues are equal and the third one differs, the point is a double degenerate point, and if all eigenvalues are the same, the point is called a triple degenerate point (alias isolated point). Besides the multiplicity, tensors are characterized by their *shape* [WPG*97]. Assuming sorted eigenvalues $\lambda_1 \geq \lambda_2 \geq \lambda_3$, a tensor is linear if $\lambda_1 > \lambda_2 \simeq \lambda_3$, or planar if $\lambda_1 \simeq \lambda_2 > \lambda_3$ is valid. A tensor is called neutral if the intermediate eigenvalue is the average of the major eigenvalue and the minor eigenvalue, and it is called isotropic if $\lambda_1 = \lambda_2 = \lambda_3$ applies. There is no well-defined analogy to separatrices in three dimensions. However, Tricoche et al. [THBG12] presented an alternative to separatrices in the two- and three-dimensional case. Therefore, they applied Lagrangian coherent structures based on the finite-time Lyapunov exponent to eigenvector tensor field topology.

Three-dimensional tensor field topology was first investigated by Zheng et al. [ZP04, ZPP05]. They showed that double degenerate points form lines in general. The extraction of those lines is numerically challenging and has been identified as one of the main problems. After this first work, there was not much activity in further developing three-dimensional tensor topology until recently the number of related publications increased.

Palacios et al. [PYW*13, PYW*16] introduced feature surfaces complementing degenerate lines. These are neutral surfaces, separating linear and planar tensors, and traceless surfaces, separating tensors with positive and negative trace. An important contribution towards a three-dimensional tensor field topology is the work on linear tensor fields by Zhang et al. [ZTZ15], which is a precondition for dealing with more general fields. They prove that under the assumption of structurally stable conditions, there are at least one and at most four degenerate curves, ending at infinity. In a follow up work, they also give an estimate of the maximum number of transition points on degenerate curves, where the tensor behavior switches from linear to planar [ZRSZ18]. Additionally, they show the existence of degenerate loops and intersections of degenerate loops of the same type. Even with these advances, Zhang and Zhang [ZZ15] summarized many remaining challenges and grouped them in three classes:

- Fundamental concept developments: Semantic parameterization of tensors for three-dimensional tensor fields similar to the two-dimensional case; Controlled simplification of tensor field topology based on a three-dimensional index theory; Relation of three-dimensional tensor fields and their projections.
- Algorithmic challenges: Stable and efficient extraction and classification of degenerate curves and feature surfaces.
- Interpretation in physical applications: Impact of triple degenerate points, wedges, trisectors, and transition points.

Roy et al. [RKZZ19] targeted the problem of a robust extraction of degenerate lines. They proposed an algorithm based on a novel parameterization of the degenerate curves and neutral surfaces, resulting in a more robust and efficient computation. This extraction method is based on the fact that degenerate points of three-dimensional linear tensor fields are diffeomorphic to ellipses and neutral points are diffeomorphic to the real projective space with a handle attached. To demonstrate the advantages, they applied their techniques to simulation data from solid mechanics. Together with their approach, Qu et al. [QRZZ20] developed a new approach for the seamless extraction of mode surfaces based on the work of Palacios et al. [PYW*16]. These surfaces are a generalization of degenerated curves and neutral surfaces. The core of the approach is their novel topological analysis of mode surfaces. They applied it to stress tensor fields from solid mechanics in order to optimize them for their pressure behavior.

Zobel and Scheuermann [ZS18] introduced a different perspective on topological features in tensor analysis. They define so-called extreme points of the tensor field as points where the gradient of the invariant map has a lower rank. This leads to extremal lines in two-dimensional domains and extremal surfaces in three-dimensional domains. The extremal point set contains the degenerate points and can, therefore, be seen as an extension.

Oster et al. [ORT18] introduced another topological line, the tensor core line. They adapted vortex core methods from flow fields to tensor fields by using the eigenvectors. This core line functions as an axis indicate swirling behavior around it.

Tensor fields are well suited to describe textures for three-dimensional objects and tensor field topology has also been used in this context. Palacios et al. [PMC*16, PRK*17] presented an interactive three-dimensional tensor field design system that allows to locally edit the topology of the three-dimensional tensor field. Roy et al. [RKG*17] introduced an interactive design and visualization system for the Branched Covering Space (BCS) of a manifold surface to review the topological structure. This system offers users the opportunity to intuitively explore the properties of BCSs using various visualization and mesh deformation techniques.

8.3. Topology simplification

Topological simplification is a key property when applying topological analysis in real-world applications. Since the introduction of tensor field topology, there has been significant work in this direction, for example, see Tricoche [Tri02] and Auer [Aue13]. Since Kratz et al. [KASH13] already discussed their work, we refer to their survey for more details.

More recently, Wang and Hotz [WH17] presented a measure for the stability of degenerate points in relation to small disturbances of the field. The measurement is based on the concept of robustness and well group theory. By extending this concept to two-dimensional symmetric second-order tensor fields, a basis for hierarchical-based tensor field topology simplification was created. Jankowai et al. [JWH19] extended this work by presenting a computational pipeline for generating a hierarchical set of degenerate points, indicating their likelihood to cancel at field perturbation.

8.4. Combinatorial line field topology

In recent work, Lewiner et al. [LNPT17] and Novello et al. [NPTL20] opened a novel perspective on the topic of two-dimensional line field topology. Based on the concepts by Forman [For98] on discrete vector fields, they introduced a topological approach for the decomposition of discrete line fields. They also introduced a topologically consistent cancellation of critical elements. Since line fields show a strong relation to eigenvector fields this could also open new possibilities for tensor field topology.

8.5. Two-dimensional asymmetric second-order tensor fields

For asymmetric tensor fields, the structure is more versatile than for symmetric tensor fields and the theory is less developed. Typically, asymmetric tensors are decomposed in their symmetric and asymmetric part, which are then treated separately. Another way is to consider the two-dimensional, asymmetric tensor as a whole and decompose the domain based on its eigenvalues in two parts: The *real part*, where the tensor has two real eigenvalues and shear dominates, and the *complex part*, where the tensor has a pair of complex conjugate eigenvalues and rotation dominates. Different from the symmetric case, the eigenvectors in the real part are not necessarily orthogonal to each other. In complex domains, no real eigenvectors exist, however, continuous extensions of eigenvectors have been introduced. One example are the dual eigenvectors by Zheng and Pang [ZP05] that are used to define a topological structure in the complex parts of asymmetric tensor fields. Palke et al. [PLC*11] defined a reparameterization of the tensors leading to the notions of an eigenvalue manifold and an eigenvector manifold. A nice feature of this parameterization is that it carries the physical meaning of the tensor components and thus can be directly used for effective visualizations. One example is the illustrative visualization of tensor fields by Auer et al. [AKK*13].

Building on the tensor parameterization, Lin et al. [LYLZ12] defined two topological graphs for two-dimensional asymmetric tensor fields: an eigenvector graph and an eigenvalue graph. The graphs are based on a segmentation of the domain with respect to the tensor type derived from a partitioning of the eigenvalue and eigenvector manifold. The eigenvector graph considers two distinguishing features forming four types of regions divided into real or complex regions and clockwise or counterclockwise rotational flow. The eigenvalue graph uses five types of regions: positive isotropic scaling, negative isotropic scaling, counterclockwise rotation, clockwise rotation, and anisotropic stretching. The nodes of the graphs are built from the resulting feature regions and the edges describe their adjacency relations. Khan et al. [KRZ*19] provide a novel multiscale topological analysis framework for asymmetric tensor fields on surfaces based on these concepts of eigenvalue and eigenvector graphs. An example can be found in Figure 15, where the eigenvalue graph of a diesel engine is shown.

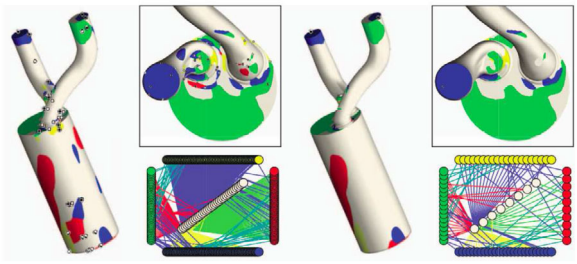

Figure 15: *Diesel engine - eigenvalue graph of the gradient tensor (left), eigenvalue graph after simplification (right) (image from [KRZ*19]).*

9. Tensor as Multivariate Entity

In some applications, tensors are not treated as one entity but rather as a set of scalars and vectors. The scalars are typically tensor invariants, e.g., eigenvalues, and their related directions. Which of these attributes are relevant is application-specific as it depends on the tensor's semantic. The attributes span an attribute space which itself can be considered as multifield and typical multifield visualization techniques may be applied [KH13]. The following section aims to give a brief overview of such methods that have previously been employed within tensor visualization, as a comprehensive literature review of multivariate data visualization would far exceed the scope of this survey.

Volume Rendering – Kindlmann et al. [KWH00] introduced Direct Volume Rendering (DVR) of diffusion tensor data considering more than one scalar tensor invariant. They define a transfer function within the barycentric space of isotropy, linear anisotropy, and planar anisotropy. Barycentric (opacity) transfer functions assign an opacity value to each location inside this shape space. The transfer function can then be sampled by calculating the barycentric coordinates for every tensor, assigning the corresponding opacity value to that voxel. Fuchs and Hjelmervik [FH15] used an approach to directly visualize mechanical stress in the three-dimensional space using interactive DVR.

Dick et al. [DGBW10] developed a volumetric visualization of stress tensors for implant design. They combine tensor lines for the major eigenvector and the minor eigenvector fields with volume rendering. Therefore, they introduced a color mapping that distinguishes between compressive and tensile forces.

Attribute space interaction and analysis – There have been other efforts to combine directional and scalar information using hybrid rendering. For an interactive exploration of tensor data, Kratz et al. [KMH11] proposed to link feature space plots with three-dimensional hybrid visualizations. They used the invariant space as a basis. Brushing and linking techniques are used to select features of interest for a hybrid visualization. Thereby, volume rendering serves as context and glyphs and tensor lines are used to add more details. The work by Jankowai et al. [JSJ*20] extended this work using hierarchical attribute space clustering, treemaps, and glyph based legends for interaction. Another approach to investigate attribute spaces are fiber surfaces [CGT*15, RBN*19, BRS*19, RBR*20, BRP*20] (see Section 6).

Attribute space clustering has also been applied by Dobrec et al. [DLL11] for interactive visual analysis of volumetric data. The user interacts with an abstract cluster tree to assign material properties to the clusters, thus highlighting attributes of interest. Additional attribute space clustering approaches have been demonstrated by Cay et al. [CNCO17] and Wang et al. [WZL*12].

In context with attribute space representations of tensor fields, Massood and Hotz [MH19] presented an accurate derivation of the contour spectrum for tensor invariants with quadratic behavior computed from two-dimensional piece-wise linear tensor fields.

Feature-based analysis – An alternative to explorative interaction with the attribute space is the targeted formulation and querying of features. Feature level-sets offer a framework wherein the user can define a feature through geometries in attribute space [JH18]. These geometries, called traits, are the image of the feature level-sets in attribute space. A distance field, describing the distance to the closest trait, is then projected back into the domain, where a simple DVR approach or marching cubes can be used to visualize the corresponding feature level-sets.

Heat Kernel Signature (HKS) offers a different approach to feature definition. HKS is typically used as a shape descriptor for surfaces, albeit not restricted to surfaces but valid for arbitrary Riemannian manifolds. It assigns a time-dependent function of the form $[0, \infty) \rightarrow \mathbb{R}$ to every point on the surface, thusly allowing a comparison of the surface for different time steps. Zobel et al. [ZRH14] first applied the concept to positive definite tensor fields and later extended their work to indefinite tensors, such as the stress tensor [ZRH15]. They achieved this by using three different mappings applied to the eigenvalues of tensors, without changing the eigenvectors. The HKS method is sensitive to the derivative of the tensor. Thus, it encodes more information than other methods. The time parameter supports a level of detail analysis.

Pattern matching – Hlawitschka et al. [HES04] defined the Fourier transform, convolution, and correlation for second-order tensor fields. Additionally, they presented pattern matching based on that work and since the convolution theorem holds, they stated the availability of Fast Fourier transform algorithms for efficient calculations.

Bujack and Hagen [BH17] defined rotation invariant moments for tensors of any order in two and three dimensions. These invariant moments allow defining patterns of interest and the employment of pattern matching techniques to query the data.

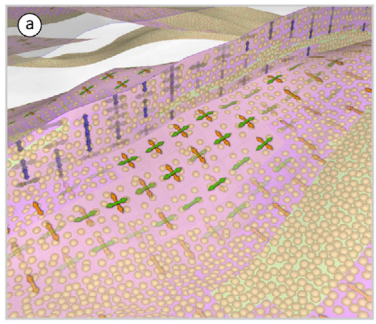

Figure 16: *Multivariate visualization of an oil reservoir showing the permeability tensor as well as the rock type and the porosity (image from [RMH*18]).*

Tensors as part of a multifield – Tensors also occur alongside with other fields in a multifield setting. An example from geology is the investigation of the structure and the permeability of rock [BDLG15] or the estimation of the most suitable locations of wells for carbohydrate reservoirs [RMH*18]. The permeability tensor appears in conjunction with other geological attributes, like rock type (categorical data), porosity (scalar data), and oil saturation (scalar data) (see Figure 16). In Rocha's work, the data is visualized by combining layered colored surfaces and glyphs while applying illustrative effects or using their so-called decal-mapping techniques [RASS17]. This technique maps two-dimensional texture quads onto arbitrarily curved surfaces without the well-known problems of clipping or detachment of these glyphs.

Rocha et al. [RSA*18] continued their work on multivariate visualization techniques for geological problems and invented a new lens technique. They used these lenses to superimpose the shown data on the surface with other attributes, like detail on-demand visualizations. The interactive placement, attribute selection, and the customizability of the size of their lenses facilitates the analysis of the relation between the vast amount of attributes.

Wünsche et al. [WY03, WLY04] developed a visualization framework to improve the understanding of cardiac mechanics. Their framework utilizes glyphs, hyperstreamlines, isosurfaces, textures, and color-coding to analyze myocardial strain and displacements embedded in a schematic drawing of a heart. Chitiboi et al. [CA17] and Sheharyar et al. [SCK*16] represented a review of current approaches for the visualization of magnetic resonance imaging of myocardial strain. Most visualizations facilitate the conventional AHA bulls-eye plot to generate a two-dimensional map of the left ventricle [CWD*02]. Strain, deformation, and other parameters are visualized on this map using color, arrows, or glyphs. Takayama et al. [TIHN07] designed a sketch-based interface for modeling a myocardial volumetric fiber orientation field. The resulting line field is used as input for reliable simulations of the heart. Teixeira et al. [TNKW20] developed an integrative mechanobiological framework for modeling intracranial aneurysm stability and growth. They combined visualizations of the aneurysm geometry, streamlines representing the flow, and color for derived scalars from the wall properties as fiber directions, displacements, and strain. Walton et al. [WBT*14] proposed a multilayered visualization con-

cept for time-varying multifields derived from Cardiovascular Magnetic Resonance (CMR) imaging data. The data includes a motion vector field, strain tensors for each time step, and multiple other attributes, e.g., density and voxel classification. They visualized these attributes using a color or encoded them into multivariate glyphs.

10. Observations and Insights

Table 1 summarizes the appearance of tensors and their visualizations in the discussed application areas. Therefore, it can be seen that some of the tensors, like the stress or the strain tensor, are relevant in multiple areas. Thus, the application areas share some of their challenges and visualization methods. Other tensors, like the moment tensor, are application-specific and require specialized visualization methods. The table also shows, that most visualizations are designed for a specific tensor type, and since the survey of Kratz et al. [KASH13] still most methods in all three areas are glyph-based.

A relatively new, slowly developing topic since 2013 is the use of tensor topology visualization in practice. First publications in this direction are encouraging and give hope for more real-world applications of tensor topology. All together, increasing activity in fundamental research is observable. Thereby, a remaining challenging question is the controlled simplification of tensor fields, especially in three dimensions.

It is apparent that papers using complex visualizations are mostly published in the visualization community. In the domain, experts mainly use simple visualization methods, like isosurfaces and color mapping. One exception is the visualization of the moment tensor. A large set of more or less complex glyphs have been introduced in the domain and are commonly used. This development is hardly acknowledged by the visualization community, where only one paper exists that visualizes the moment tensor. In biomechanics also a greater variety of complex visualization techniques are used in the domain. However, these are mostly basic methods combined in an application-specific way. Looking into papers from the visualization community in general, not many papers focus on geomechanical problems. Even if some of the appearing tensors, like the stress and strain tensor, are the same as in the other discussed domains, only a few works are discussing geomechanical applications. Many more papers in the visualization community deal with applications from structural mechanics and biomechanics. In structural mechanics, visualizations of the stress and the strain tensor are prevalent. Other tensors are commonly visualized by glyphs.

The dominance of stress and strain tensors could be related to the fact that they are relatively simple, symmetric, second-order, and well understood. They appear in many areas of application. In contrast, higher-order tensors are not well understood. No basic decompositions exist, and a clear intuition is missing. Only a few tensors, like the stiffness tensor, are visualized in some works since 2013, but we could not find papers focusing on visualizations of higher-order tensors with geomechanical examples. It is unclear whether higher-order tensors are not significant for geomechanical applications or if these tensors are just not visualized. Gradients are also rarely visualized even though they are obviously of interest, e.g., the predominant stresses at a specific point have a bearing on the failure of components as well as the distribution of stress in different directions. The field of asymmetric second-order tensors was hardly touched since Kratz et al. [KASH13] except by a few theoretical visualization papers. Asymmetric tensors are, in general, decomposed into their symmetric and antisymmetric parts and analyzed separately. The deformation gradient tensor may have potential applications in all areas of mechanics. Additionally, it is noticeable that most of the used data sets are from simulations or imaging because the direct measuring of most tensors is difficult. An exception are the moment tensor data sets, which are acquired by the inversion of received seismic waves, but these measurements are sparse in space and time.

Section 2 described the different areas of the application domains discussed in this survey. It can be seen that the abstract questions in mechanical engineering, bio-, and geomechanics are very similar. Their foci are on the detection of critical areas and the analysis of a material's responce to external influences. Even if the materials are different, the considered tensors are the same. In mechanical engineering, the synthesis of anisotropic materials and their application for technical purposes is in the foreground. In contrast, bio- and geomechanics are more concerned with identifying the structure and properties of natural material. A specific challenge with biomaterials, e.g., soft tissues and muscles, is their dynamical behavior with largely changing geometry, for example, the heart.

As a consequence of unknown properties of materials or loading conditions, uncertainty in simulation models and their parameterization becomes a dominant issue in model-based decision making. There are some papers published since the survey of Kratz et al. [KASH13], which visualize uncertainty tensors to analyze the distribution in tensor ensembles. However, these works are restricted to unimodal distributions of tensor ensembles, liable to a Gaussian distribution. There exist no publications looking at multimodal distributions and other distributions so far. Uncertainty quantification and visualization still provide many challenging questions.

Another interesting aspect is that of spatial and temporal scale. Geological processes are evolving over geological time and are influenced by processes on scales ranging from microscopic properties to tectonic plates. In biological material, scales are ranging from the molecular level up to organs. Analyses bridging these scales constitute a challenge for visualization finding the right abstraction levels, particularly since the scales may be beyond human intuition.

Not often discussed visualizations, in general, are comparative visualizations. They are neither used for different material models nor different visualization designs. By now, this is done in most cases by juxtaposition, i.e., comparing two separate visualizations side by side.

A general observation is that many of the methods developed in the visualization community are not well-known by the domain experts. One reason might be that domain experts have no access to such methods since they are not provided by common visualization frameworks, like ParaView. Another reason might be a missing tradition in using advanced visualizations. In any case, all three fields considered in this survey provide a large potential for novel visualization research. Thereby, an increased effort in reaching out to the domain scientists is necessary.

10.1. Future work and open questions

These discussed results lead to some open questions and accordingly to starting points for future research:

- There are some underrepresented tensors types, like higher-order, uncertainty, ensembles, or gradients. For their analysis and visualization, it would be interesting to investigate the transferability of methods from other application areas.
- For the visualization of higher-order tensors, to reach more applications would be interesting. A major challenge is to find ways to encode all the tensor information in an intuitive way.
- Visualization of uncertainty inside the data and the used models is an important, however strongly underrepresented, topic.
- Considering tensor topology, there is still a lot of fundamental research to do, with respect to improving extraction methods for the three-dimensional case and developing generic simplification strategies. Furthermore, real-world applications are still missing. A major task is to relate topological features with the driving questions in the applications.
- There are some domains that have not been discovered by the visualization community, e.g., the moment tensor, although visualization is commonly used in the domain. A major hurdle here is the communication barrier due to the domain language.
- The implementation of existing methods into well-known visualization frameworks to bring them more into the range of scientists. This entails an expansion of existing methods to more complex domains, geometries, and data structures.

11. Conclusion

A résumé about the tensor visualizations in three selected application areas: mechanical engineering, bio-, and geomechanics is given by this survey. It is structured in three main sections. At first, a description of the applications, followed by a summary of the mathematical foundations, and the visualization methods, grouped by the type of visualization. In the end, the gained insights about the visualizations in relation to the application domains are given.

Going back to the purpose of this survey as formulated in Section 1: (a) *Highlight the usefulness and applicability of tensor analysis within the three fields.* This is obvious regarding the vast amount of papers with successful applications. However, one can also observe that these papers are mostly published inside the visualization community. Domain-specific publications often do not use these techniques and rather use simple or their own techniques. (b) *The accent of the essential differences in-between them*. Even though the three fields have common grounds, the used visualization techniques are mostly restricted to one application area and only some techniques are used across the domains.

Summarizing the findings of this survey, it can be said, there exist only a few general generic methods to visualize tensors. Many visualization methods are mainly used in a specific context, like beach balls for moment tensors, even though they might also be interesting for other applications or for visualization experts, to show how others attempt to process tensor data into images. Simple methods as glyph representations are the most prevalent technique in all discussed domains. This could be an indication that glyphs are more intuitive. There seems to be some skepticism towards more advanced methods, like volume rendering, exploration, or attribute space visualization methods. Often such methods are not very well known in the user's domains. Here, we probably need more outreach and promotion, not only to the domain scientists but also to the visualization tool makers. There are also many remaining challenges in the field, ranging from fundamental to applied questions. As a closing remark, we encourage any visualization researchers approaching new applications in tensor visualization, to also look into other domains and inspect their approaches with respect to transferability.

Acknowledgment

Open access funding enabled and organized by Projekt DEAL.

References

[AAC*19] Ambrosi D., Amar M. B., Cyron C. J., DeSimone A., Goriely A., Humphrey J. D., Kuhl E.: Growth and remodelling of living tissues: Perspectives, challenges and opportunities, Aug 2019.

[AJL*19] Arora R., Jacobson A., Langlois T. R., Huang Y., Mueller C., Matusik W., Shamir A., Singh K., Levin D. I.: Volumetric michell trusses for parametric design & fabrication. In *Proceedings of the ACM Symposium on Computational Fabrication* (2019), ACM, p. 6.

[AKK*13] Auer C., Kasten J., Kratz A., Zhang E., Hotz I.: Automatic, tensor-guided illustrative vector field visualization. In *Proceedings of IEEE PacificVis Conference* (2013), pp. 265–275.

[ASKH12] Auer C., Stripf C., Kratz A., Hotz I.: Glyph- and texture-based visualization of segmented tensor fields. In *International Conference on Information Visualization Theory and Applications (IVAPP'12)* (2012).

[ASKT18] Alvizuri C., Silwal V., Krischer L., Tape C.: Estimation of full moment tensors, including uncertainties, for nuclear explosions, volcanic events, and earthquakes. *Journal of Geophysical Research: Solid Earth 123*, *6* (2018), 5099–5119.

[Aue13] Auer C.: *Visualization of fundamental structures in two dimensional second order tensor fields on planar and curved surfaces*. PhD thesis, Free University Berlin, 2013.

[AWHS15] Abbasloo A., Wiens V., Hermann M., Schultz T.: Visualizing tensor normal distributions at multiple levels of detail. *IEEE Transactions on Visualization and Computer Graphics 22*, *1* (2015), 975–984.

[Aya15] Ayachit U.: *The ParaView Guide: A Parallel Visualization Application*. Kitware, Inc., 2015.

[Bac70] Backus G.: A geometrical picture of anisotropic elastic tensors. *Reviews of Geophysics 8*, *3* (1970), 633–671.

[BB01] Böhlke T., Brüggemann C.: Graphical representation of the generalized Hooke's law. *Technische Mechanik 21*, *2* (2001), 145–158.

[BDLG15] Boyd O. S., Dreger D. S., Lai V. H., Gritto R.: A systematic analysis of seismic moment tensor at the geysers geothermal field, California. *Bulletin of the Seismological Society of America 105*, *6* (2015), 2969–2986.

[BES15] Bußler M., Ertl T., Sadlo F.: Photoelasticity raycasting. *Computer Graphics Forum 34*, *3* (2015), 141–150.

[BH17] Bujack R., Hagen H.: Moment invariants for multi-dimensional data. In *Modeling, Analysis, and Visualization of Anisotropy* (2017), Schultz T., Özarslan E., Hotz, I. (Eds.), Springer, pp. 43–64.

[BHA*15] Bhattacharya A., Heinzl C., Amirkhanov A., Kastner J., Wenger R.: MetaTracts – A method for robust extraction and visualization of carbon fiber bundles in fiber reinforced composites. In *2015 IEEE Pacific Visualization Symposium (PacificVis)* (2015), IEEE, pp. 191–198.

[BHC*19] Bishop P. J., Hocknull S. A., Clemente C. J., Hutchinson J. R., Farke A. A., Beck B. R., Barrett R. S., Lloyd D. G.: Cancellous bone and theropod dinosaur locomotion. Part I–An examination of cancellous bone architecture in the hindlimb bones of theropods. *PeerJ 6* (Oct 2019), e5778.

[BL14] Böhlke T., Lobos M.: Representation of Hashin–Shtrikman bounds of cubic crystal aggregates in terms of texture coefficients with application in materials design. *Acta Materialia 67* (2014), 324–334.

[Boy18] Boyd O. S.: *Analysis of Seismic Moment Tensors, In-Situ Stress, and Finite-Source Scaling of Earthquakes at The Geysers Geothermal Field, California*. PhD thesis, UC Berkeley, 2018.

[BP98] Boring E., Pang A.: Interactive deformations from tensor fields. In *Proceedings Visualization'98 (Cat. No. 98CB36276)* (1998), IEEE, pp. 297–304.

[BRP*20] Blecha C., Raith F., Präger A. J., Nagel T., Kolditz O., Maßmann J., Röber N., Böttinger M., Scheuermann G.: Fiber surfaces for many variables. *Computer Graphics Forum 39*, *3* (2020), 317–329.

[BRS*19] Blecha C., Raith F., Scheuermann G., Nagel T., Kolditz O., Maßmann J.: Analysis of coupled thermo-hydro-mechanical simulations of a generic nuclear waste repository in clay rock using fiber surfaces. In *2019 IEEE Pacific Visualization Symposium (PacificVis)* (April 2019), pp. 189–201.

[BUM*12] Baig A., Urbancic T. I., Mace K. C., Prince M., et al.: Assessing the spacing of stages in plug-and-perf completions through seismic moment tensor inversion. In *SPE Hydraulic Fracturing Technology Conference* (2012), Society of Petroleum Engineers.

[BWW*17] Bhattacharya A., Weissenböck J., Wenger R., Amirkhanov A., Kastner J., Heinzl C.: Interactive exploration and visualization using metatracts extracted from carbon fiber reinforced composites. *IEEE Transactions on Visualization and Computer Graphics 23*, *8* (2017), 1988–2002.

[BYDS19] Bi C., Yang L., Duan Y., Shi Y.: A survey on visualization of tensor field. *Journal of Visualization* (Mar 2019).

[CA17] Chitiboi T., Axel L.: Magnetic resonance imaging of myocardial strain: a review of current approaches. *J. Magn. Reson. Imaging 46* (2017), 1263–1280.

[CGT*15] Carr H., Geng Z., Tierny J., Chattopadhyay A., Knoll A.: Fiber surfaces: generalizing isosurfaces to bivariate data. *Computer Graphics Forum 34*, *3* (2015), 241–250.

[CL12] Chapman C. H., Leaney W. S.: A new moment-tensor decomposition for seismic events in anisotropic media. *Geophysical Journal International 188*, *1* (2012), 343–370.

[CNCO17] Cai L., Nguyen B. P., Chui C.-K., Ong S.-H.: A two-level clustering approach for multidimensional transfer function specification in volume visualization. *The Visual Computer 33* (2017), 163–177.

[CnMMM*09] Cammoun L., no Moraga C. A. C., Munoz-Moreno E., Sosa-Cabrera D., Acar B., Rodriguez-Florido M. A., Brun A., Knutsson H., Thiran J. P.: A review of tensors and tensor signal processing. In *Tensors in Image Processing and Computer Vision* (2009), Aja-Fernandez S., de Luis Garcia R., Tao D., Li X., (Eds.), vol. 1 of *Advances in Pattern Recognition*. Springer London Ltd.

[Cro04] Cronin V.: A Draft Primer on Focal Mechanism Solutions for Geologists. *Texas. Baylor University* (2004).

[CUS*15] Cladouhos T. T., Uddenberg M., Swyer M. W., Petty S., Nordin Y.: Production well targeting at newberry volcano EGS demonstration. *GRC Transactions 39* (2015).

[CWD*02] Cerqueira M. D., Weissman N. J., Dilsizian V., Jacobs A. K., Kaul S., Laskey W. K., Pennel D. J., Rumberger J., Ryan T. J., Verani M. S.: Standardized myocardial segmentation and nomenclature for tomographic imaging of the heart. *Journal of Cardiovascular Magnetic Resonance 4*, 2 (2002), 203–210.

[DGBW10] Dick C., Georgii J., Burgkart R., Westermann R.: Stress tensor field visualization for implant planning in orthopedics. *IEEE Transactions on Visualization and Computer Graphics 15* (01 2010), 1399–406.

[DH92] Delmarcelle T., Hesselink L.: Visualization of second order tensor fields and matrix data. In *Proceedings Visualization '92* (Oct 1992), pp. 316–323.

[DH93] Delmarcelle T., Hesselink L.: Visualizing second-order tensor fields with hyperstreamlines. *IEEE Computer Graphics and Applications 13*, 4 (July 1993), 25–33.

[DH94] Delmarcelle T., Hesselink L.: The topology of symmetric, second-order tensor fields. In *Proceedings Visualization'94* (1994), IEEE, pp. 140–147.

[Dic89] Dickinson R. R.: A unified approach to the design of visualization software for the analysis of field problems. In

Three-Dimensional Visualization and Display Technologies (1989), Fisher S. S., Robbins W. E., (Eds.), vol. 1083, International Society for Optics and Photonics, SPIE, pp. 173–180.

[DLL11] Dobrev P., Long T. V., Linsen L.: A cluster hierarchy-based volume rendering approach for interactive visual exploration of multi-variate volume data. In *Vision, Modeling, and Visualization (2011)* (2011), Eisert P., Hornegger J., Polthier K. (Eds.), The Eurographics Association.

[Dog00] Doghri I.: Mechanics of deformable solids: Linear, nonlinear, analytical, and computational aspects. *Springer-Verlag. DOI 10* (2000), 978–3.

[DP08] De Paor D.: Enhanced visualization of seismic focal mechanisms and centroid moment tensors using solid models, surface bump-outs, and Google Earth. *Journal of the Virtual Explorer 29*, 2 (2008).

[DSB*19] Doste R., Soto-Iglesias D., Bernardino G., Alcaine A., Sebastian R., Giffard?Roisin S., Sermesant M., Berruezo A., Sanchez-Quintana D., Camara O.: A rule-based method to model myocardial fiber orientation in cardiac biventricular geometries with outflow tracts. *International Journal for Numerical Methods in Biomedical Engineering 35*, 4 (Apr 2019), e3185.

[DT06] Doghri I., Tinel L.: Micromechanics of inelastic composites with misaligned inclusions: numerical treatment of orientation. *Computer Methods in Applied Mechanics and Engineering 195*, 13 (2006).

[EHHS12] Eichelbaum S., Hlawitschka M., Hamann B., Scheuermann G.: Fabric-like visualization of tensor field data on arbitrary surfaces in image space. In *New Developments in the Visualization and Processing of Tensor Fields*. Springer, 2012, pp. 71–92.

[EKH*04] Ennis D. B., Kindlmann G., Helm P., Rodriguez I., Wen H., McVeigh E.: Visualization of high-resolution myocardial strain and diffusion tensor using super-quadric glyphs. In *Conference Proceedings of ISMRM* (2004).

[FH15] Fuchs F. G., Hjelmervik J. M.: Interactive isogeometric volume visualization with pixel-accurate geometry. *IEEE Transactions on Visualization and Computer Graphics 22*, 2 (2015), 1102–1114.

[FHHJ08] Feng L., Hotz I., Hamann B., Joy K.: Anisotropic noise samples. *IEEE Transactions on Visualization and Computer Graphics 14*, 2 (2008), 342–354.

[FKGR03] Finck F., Kurz J. H., Grosse C. U., Reinhardt H.-W.: Advances in moment tensor inversion for civil engineering. In *International Symposium on Non–Destructive Testing in Civil Engineering* (2003).

[FL96] Fu S.-Y., Lauke B.: Effects of fiber length and fiber orientation distributions on the tensile strength of short-fiber-reinforced polymers. *Composites Science and Technology 56*, 10 (1996).

[For98] Forman R.: Combinatorial vector fields and dynamical systems. *Mathematische Zeitschrift 228*, 4 (1998), 629–681.

[Gao18] Gao X.: Applying 2D Tensor Field Topology to Symmetric Stress Tensors (2018).

[GD11] Guilhem A., Dreger D. S.: Rapid detection and characterization of large earthquakes using quasi-finite-source Green's functions in continuous moment tensor inversion. *Geophysical Research Letters 38*, 13 (2011).

[GDMS*15] Ghazanfari S., Driessen-Mol A., Strijkers G. J., Baaijens F. P. T., Bouten C. V. C.: The evolution of collagen fiber orientation in engineered cardiovascular tissues visualized by diffusion tensor imaging. *PLOS ONE 10*, 5 (May 2015), e0127847.

[Gil71] Gilbert F.: Excitation of the normal modes of the earth by earthquake sources. *Geophysical Journal International 22*, 2 (02 1971), 223–226.

[GM09] Grytz R., Meschke G.: *Microstructure-Oriented Modeling and Computational Remodeling of the Collagen Network in Corneo-Scleral Shells*. Springer Netherlands, Dordrecht, 2009, pp. 155–168.

[GNK12] Gannon A., Nagel T., Kelly D.: The role of the superficial region in determining the dynamic properties of articular cartilage. *Osteoarthritis and Cartilage 20*, 11 (Nov 2012), 1417–1425.

[GRT17] Gerrits T., Rössl C., Theisel H.: Glyphs for general second-order 2D and 3D tensors. *IEEE Transactions on Visualization and Computer Graphics 23*, 1 (2017), 980–989.

[GRT19] Gerrits T., Rössl C., Theisel H.: Towards glyphs for uncertain symmetric second-order tensors. *Computer Graphics Forum 38*, 3 (2019), 325–336.

[GYLG20] Guan D., Yao J., Luo X., Gao H.: Effect of myofibre architecture on ventricular pump function by using a neonatal porcine heart model: from DT-MRI to rule-based methods. *Royal Society Open Science 7*, 4 (Apr 2020), 191655.

[HBGW20] Hotz I., Bujack R., Garth C., Wang B.: *Mathematical Foundations in Visualization*. Springer International Publishing, Cham, 2020, pp. 87–119.

[Hel15] Helbig K.: *Foundations of Anisotropy for Exploration Seismics: Section I. Seismic Exploration*, vol. *22*. Elsevier, 2015.

[HES04] Hlawitschka M., Ebling J., Scheuermann G.: Convolution and fourier transform of second order tensor fields. *Proceedings of IASTED VIIP 2004* (2004), 78–83.

[HFH*04] Hotz I., Feng L., Hamann B., Joy K., Jeremić B.: Physically based methods for tensor field visualization. In *IEEE Visualization 2004* (11 2004), pp. 123–130.

[HFH*05] Hotz I., Feng L., Hamann B., Manaker D., Conjeepuram N., Kellogg L. H., Billen M. I.: Exploring tensor

fields using a fabric like texture on arbitrary surfaces. In *AGU Fall Meeting San Francisco*, CA, USA (2005).

[HFH*06] Hotz I., Feng L., Hagen H., Hamann B., Joy K.: Tensor field visualization using a metric interpretation. In *Visualization and Processing of Tensor Fields*. Springer, 2006, pp. 269–281.

[HH00] Higham D. J., Higham N. J.: *MATLAB Guide*. Citeseer, 2000.

[HKS98] Hibbett, Karlsson, Sorensen: *ABAQUS/standard: User's Manual*, vol. 1. Hibbitt, Karlsson & Sorensen, 1998.

[HLH*16] Heine C., Leitte H., Hlawitschka M., Iuricich F., De Floriani L., Scheuermann G., Hagen H., Garth C.: A Survey of topology-based methods in visualization. *Computer Graphics Forum 35*, 3 (2016), 643–667.

[HLL97] Hesselink L., Levy Y., Lavin Y.: The topology of symmetric, second-order 3D tensor fields. *IEEE Transactions on Visualization and Computer Graphics 3*, 1 (1997), 1–11.

[HNKS19] Hergl C., Nagel T., Kolditz O., Scheuermann G.: Visualization of symmetries in fourth-order stiffness tensors. In *2019 IEEE Visualization Conference (VIS)* (2019), IEEE, pp. 291–295.

[HNS20] Hergl C., Nagel T., Scheuermann G.: An introduction to the deviatoric tensor decomposition in three dimensions and its multipole representation.

[Hol00] Holzapfel G.: *Nonlinear Solid Mechanics*, Vol. *24*. Chichester, New York, 2000.

[HPR89] Hudson J., Pearce R., Rogers R.: Source type plot for inversion of the moment tensor. *Journal of Geophysical Research: Solid Earth 94*, B1 (1989), 765–774.

[HS17] Heinzl C., Stappen S.: STAR: visual computing in materials science. *Computer Graphics Forum 36*, 3 (2017), 647–666.

[HWS*19] Hasaballa A. I., Wang V. Y., Sands G. B., Wilson A. J., Young A. A., LeGrice I. J., Nash M. P.: Microstructurally motivated constitutive modeling of heart failure mechanics. *Biophysical Journal 117*, 12 (Dec 2019), 2273–2286.

[JFK*15] Jianping C., Feng L., Kemao Q., Tsui L. Y., Soon S. H.: Simulation and visualization of deformation with anisotropic materials. In *2015 19th International Conference on Information Visualisation* (2015), IEEE, pp. 392–402.

[JH18] Jankowai J., Hotz I.: Feature level-sets: generalizing iso-surfaces to multi-variate data. *IEEE Transactions on Visualization and Computer Graphics* (2018), 1–1.

[JKLSI10] Jankun-Kelly T., Lanka Y., Swan II J.: An evaluation of glyph perception for real symmetric traceless tensor properties. *Computer Graphics Forum 29*, 3 (2010), 1133–1142.

[JKM06] Jankun-Kelly T., Mehta K.: Superellipsoid-based, real symmetric traceless tensor glyphs motivated by nematic liquid crystal alignment visualization. *IEEE Transactions on Visualization and Computer Graphics 12*, 5 (2006), 1197–1204.

[JSF*02] Jeremić B., Scheuermann G., Frey J., Yang Z., Hamann B., Joy K. I., Hagen H.: Tensor visualizations in computational geomechanics. *International Journal for Numerical and Analytical Methods in Geomechanics 26*, 10 (2002), 925–944.

[JSJ*20] Jankowai J., Skånberg R., J'onsson D., Ynnerman A., Hotz I.: Tensor volume exploration using feature space representatives. In *Proceedings of LEVIA 20* (2020).

[JWH19] Jankowai J., Wang B., Hotz I.: Robust extraction and simplification of 2D symmetric tensor field topology. *Computer Graphics Forum 38*, 3 (2019), 337–349.

[KAH14] Kratz A., Auer C., Hotz I.: Tensor invariants and glyph design. In *Visualization and Processing of Tensors and Higher Order Descriptors for Multi-Valued Data*. Springer, 2014, pp. 17–34.

[KASH13] Kratz A., Auer C., Stommel M., Hotz I.: Visualization and analysis of second-order tensors: Moving beyond the symmetric positive-definite case. *Computer Graphics Forum 32*, 1 (2013), 49–74.

[KDL*20] Kang J., Dong E., Li D., Dong S., Zhang C., Wang L.: Anisotropy characteristics of microstructures for bone substitutes andporous implants with application of additive manufacturingin orthopaedic. *Materials & Design 191* (Jun 2020), 108608.

[KGG*20] Kretzschmar V., Gillmann C., Günther F., Stommel M., Scheuermann G.: Visualization framework for assisting interface optimization of hybrid component design. In *Vision, Modeling, and Visualization* (2020), Krüger J., Niessner M., Stückler J., (Eds.).

[KGSS20] Kretzschmar V., Günther F., Stommel M., Scheuermann G.: Tensor spines – A hyperstreamlines variant suitable for indefinite symmetric second-order tensors. In *2020 IEEE Pacific Visualization Symposium (PacificVis)* (2020), IEEE, pp. 106–110.

[KH13] Kehrer J., Hauser H.: Visualization and visual analysis of multifaceted scientific data: a survey. *IEEE Transactions on Visualization and Computer Graphics (TVCG) 19*, 3 (2013), 495—513.

[KHvdH99] Kellogg L. H., Hager B. H., van der Hilst R.: Compositional stratification in the deep mantle. *Science 283* (1999), 1881–1884.

[KLC16] Kwok T.-H., Li Y., Chen Y.: A structural topology design method based on principal stress line. *Computer-Aided Design 80* (2016), 19–31.

[KMH11] Kratz A., Meyer B., Hotz I.: A visual approach to analysis of stress tensor fields. In *Scientific Visualization: Interactions, Features, Metaphors* (Dagstuhl, Germany, 2011), vol. 2 of Dagstuhl Follow-Ups, pp. 188–211.

[KNB13] Kardas D., Nackenhorst U., Balzani D.: Computational model for the cell-mechanical response of the osteocyte cytoskeleton based on self-stabilizing tensegrity structures. *Biomechanics and Modeling in Mechanobiology 12*, 1 (Jan 2013), 167–183.

[KR70] Knopoff L., Randall M. J.: The compensated linear?vector dipole: a possible mechanism for deep earthquakes. *Journal of Geophysical Research 75*, 26 (1970), 4957–4963.

[KRZ*19] Khan F., Roy L., Zhang E., Qu B., Hung S., Yeh H., Laramee R. S., Zhang Y.: Multi-scale topological analysis of asymmetric tensor fields on surfaces. *IEEE Transactions on Visualization and Computer Graphics 26*, 1 (2019), 270–278.

[KSZ*14] Kratz A., Schöneich M., Zobel V., Burgeth B., Scheuermann G., Hotz I., Stommel M.: Tensor visualization driven mechanical component design. In *Visualization Symposium (PacificVis), 2014 IEEE Pacific* (2014), IEEE, pp. 145–152.

[KW06] Kindlmann G., Westin C.-F.: Diffusion tensor visualization with glyph packing. *IEEE Transactions on Visualization and Computer Graphics (Vis '06) 12*, 5 (2006), 1329–1336.

[KWH00] Kindlmann G., Weinstein D., Hart D.: Strategies for direct volume rendering of diffusion tensor fields. *IEEE Transactions on Visualization and Computer Graphics 6*, 2 (2000), 124–138.

[KYHR05] Kriz R. D., Yaman M., Harting M., Ray A. A.: Visualization of Zeroth, Second, Fourth, Higher Order Tensors, and Invariance of Tensor Equations, 2005.

[LGSWN14] Le Gonidec Y., Sarout J., Wassermann J., Nussbaum C.: Damage initiation and propagation assessed from stress-induced microseismic events during a mine-by test in the Opalinus Clay. *Geophysical Journal International 198*, 1 (04 2014), 126–139.

[LH07] Labay K., Haeussler P. J.: 3D visualization of earthquake focal mechanisms using arcscene, 2007.

[LLP*18] Liu Q., Liu Q., Pan Y., Liu X., Kong X., Deng P.: Microcracking mechanism analysis of rock failure in diametral compression tests. *Journal of Materials in Civil Engineering 30*, 6 (2018), 04018082.

[LNPT17] Lewiner T., Novello T., Paixao J., Tomel C.: Discrete Gradient Line Fields on Surfaces. arXiv preprint arXiv:1712.08136 (2017).

[LNY*18] Lee C., Nguyen C., Yoon J., Chang H.-J., Kim S., Hoon Kim C., Li D.: Three-dimensional cardiomyocytes structure revealed by diffusion tensor imaging and its validation using a tissue-clearing technique. *Scientific Reports 8*, 1 (2018), 6640.

[LYC*14] Leaney S., Yu X., Chapman C., Bennett L., Maxwell S., Rutledge J., Duhault J.: Anisotropic moment tensor inversion and visualization applied to a dual well monitoring survey. *Canadian Society of Exploration Geophysicists Recorder 39* (2014), 48–54.

[LYLZ12] Lin Z., Yeh H., Laramee R., Zhang E.: 2D asymmetric tensor field topology. *Topological Methods in Data Analysis and Visualization II* (11 2012).

[LZY*17] Li W., Zheng A., You L., Yang X., Zhang J., Liu L.: Rib-reinforced shell structure. *Computer Graphics Forum 36*, 7 (2017), 15–27.

[MB15] Moakher M., Basser P. J.: Fiber orientation distribution functions and orientation tensors for different material symmetries. In *Visualization and Processing of Higher Order Descriptors for Multi-Valued Data*. Springer, 2015, pp. 37–71.

[MBH*08] Mohr R., Bobach T., Hijazi Y., Reis G., Steinmann P., Hagen H.: Comparative tensor visualisation within the framework of consistent time-stepping schemes. *Visualization of Large and Unstructured Data Sets* (2008).

[MGV*17] Müller H. R., Garitte B., Vogt T., Köhler S., Sakaki T., Weber H., Spillmann T., Hertrich M., Becker J. K., Giroud N., et al.: Implementation of the full-scale emplacement (FE) experiment at the Mont Terri rock laboratory. *Swiss J Geosci 110* (2017).

[MH19] Masood T. B., Hotz I.: Continuous histograms for anisotropy of 2d symmetric piece-wise linear tensor fields. arXiv:1912.00739 (2019).

[Mol18] Moldenhauer H.: Integration of direction fields with standard options in finite element programs. *Mathematical and Computational Applications 23*, 2 (2018), 24.

[MPB*14] Malecki A., Potdevin G., Biernath T., Eggl E., Willer K., Lasser T., Maisenbacher J., Gibmeier J., Wanner A., Pfeiffer F.: X-ray tensor tomography. *EPL (Europhysics Letters) 105*, 3 (2014), 38002.

[MSP16] Moreno R., Smedby Ö., Pahr D. H.: Prediction of apparent trabecular bone stiffness through fourth-order fabric tensors. *Biomechanics and Modeling in Mechanobiology 15*, 4 (Aug 2016), 831–844.

[NBJ*08] Neeman A. G., Brannon R., Jeremić B., Van Gelder A., Pang A.: Decomposition and visualization of fourth-order elastic-plastic tensors. In *Proceedings of the Fifth Eurographics/IEEE VGTC conference on Point-Based Graphics* (2008), Eurographics Association, pp. 121–128.

[Nee04] Neeman A. G.: Visualizing 3D Symmetric Moment Tensors In Oil.

[NK13] Nagel T., Kelly D. J.: The composition of engineered cartilage at the time of implantation determines the likelihood of regenerating tissue with a normal collagen architecture. *Tissue Engineering – Part A* (2013).

[NPTL20] Novello T., Paixao J. A. R., Tomei C., Lewiner T.: Discrete Line Fields on Surfaces, 2020.

[ORT18] Oster T., Rössl C., Theisel H.: Core lines in 3D second-order tensor fields. *Computer Graphics Forum 37*, 3 (2018), 327–337.

[PL20] Patel M., Laidlaw D. H.: Visualization of 3D stress tensor fields using superquadric glyphs on displacement streamlines. *IEEE Transactions on Visualization and Computer Graphics* (2020).

[PLC*11] Palke D., Lin Z., Chen G., Yeh H., Vincent P., Laramee R., Zhang E.: Asymmetric tensor field visualization for surfaces. *EEE Transactions on Visualization and Computer Graphics 17*, 11 (2011), 1979–1988.

[PMC*16] Palacios J., Ma C., Chen W., Wei L.-Y., Zhang E.: Tensor field design in volumes. In *SIGGRAPH ASIA 2016 Technical Briefs* (2016), ACM, p. 18.

[PRK*17] Palacios J., Roy L., Kumar P., Hsu C.-Y., Chen W., Ma C., Wei L.-Y., Zhang E.: Tensor field design in volumes. *ACM Transactions on Graphics (TOG) 36*, 6 (2017), 188.

[PYW*13] Palacios J., Yeh H., Wang W., Laramee R. S., Vincent P., Zhang E.: Robust Extraction and Analysis Towards Complete 3D Tensor Field Topology.

[PYW*16] Palacios J., Yeh H., Wang W., Zhang Y., Laramee R. S., Sharma R., Schultz T., Zhang E.: Feature surfaces in symmetric tensor fields based on eigenvalue manifold. *IEEE Transactions on Visualization and Computer Graphics 22*, 3 (March 2016), 1248–1260.

[QRZZ20] Qu B., Roy L., Zhang Y., Zhang E.: Mode Surfaces of Symmetric Tensor Fields: Topological Analysis and Seamless Extraction. arXiv preprint arXiv:2009.04601 (2020).

[RASS17] Rocha A., Alim U., Silva J. D., Sousa M. C.: Decal-maps: real-time layering of decals on surfaces for multivariate visualization. *IEEE Transactions on Visualization and Computer Graphics 23*, 1 (Jan 2017), 821–830.

[RBM20] Renaud S., Bouaanani N., Miquel B.: Numerical simulation of experimentally shear-tested contact specimens from existing dam joints. *Computers and Geotechnics 125* (2020), 103630.

[RBN*19] Raith F., Blecha C., Nagel T., Parisio F., Kolditz O., Günther F., Stommel M., Scheuermann G.: Tensor field visualization using fiber surfaces of invariant space. *IEEE Transactions on Visualization and Computer Graphics 25*, 1 (2019), 1122–1131.

[RBR*20] Raith F., Blecha C., Rink K., Wang W., Kolditz O., Shao H., Scheuermann G.: Visual analysis of a full-scale-emplacement experiment in the underground rock laboratory Mont Terri using fiber surfaces. *Computer Graphics Forum 39*, 3 (2020).

[RDMM12] Ronan W., Deshpande V. S., McMeeking R. M., McGarry J. P.: Numerical investigation of the active role of the actin cytoskeleton in the compression resistance of cells. *Journal of the Mechanical Behavior of Biomedical Materials 14* (Oct 2012), 143–157.

[RGBN14] Rodriguez-Gonzalez J., Billen M. I., Negredo A. M.: Non-steady-state subduction and trench-parallel flow induced by overriding plate structure. *Earth and Planetary Science Letters 401* (2014), 227–235.

[RKG*17] Roy L., Kumar P., Golbabaei S., Zhang Y., Zhang E.: Interactive design and visualization of branched covering spaces. *IEEE Transactions on Visualization and Computer Graphics 24*, 1 (2017), 843–852.

[RKZZ19] Roy L., Kumar P., Zhang Y., Zhang E.: Robust and fast extraction of 3D symmetric tensor field topology. *IEEE Transactions on Visualization and Computer Graphics 25*, 1 (2019), 1102–1111.

[RMH*18] Rocha A., Mota R. C. R., Hamdi H., Alim U. R., Sousa M. C.: Illustrative multivariate visualization for geological modelling. *Computer Graphics Forum* (2018).

[RSA*18] Rocha A. C. A., Silva J. D., Alim U. R., Carpendale S., Sousa M. C.: Decal-lenses: Interactive lenses on surfaces for multivariate visualization. *IEEE Transactions on Visualization and Computer Graphics* (2018), 1–1.

[SBWK01] Selskog P., Brandt E., Wigström L., Karlsson M.: Visualization of myocardial strain-rate tensors from time-resolved 3D cine phase contrast MRI. In *Proceedings of International of Society Magnatic Resonnance in Medicine* (2001).

[Sch11] Schultz T.: Topological features in 2D symmetric higher-order tensor fields. *Computer Graphics Forum 30*, 3 (2011), 841–850.

[SCK*16] Sheharyar A., Chitiboi T., Keller E., Rahman O., Schnell S., Markl M., Bouhali O., Linsen L.: Spatio-temporal visualization, of regional myocardial velocities. In *Eurographics Workshop on Visual Computing for Biology and Medicine* (2016), Bruckner S., Preim B., Vilanova A., (Eds.).

[SEHW02] Sigfridsson A., Ebbers T., Heiberg E., Wigström L.: Tensor field visualisation using adaptive filtering of noise fields combined with glyph rendering. In *VIS '02: Proceedings of the conference on Visualization '02* (Washington, DC, USA, 2002), IEEE Computer Society, pp. 371–378.

[Sie20] Siemens Industry Software Inc.: NX, 2020.

[SJCT20] Singh S., Miers J.C., Saldana C., Murthy T.G.: Quantification of fabric in cemented granular materials. *Computers and Geotechnics 125* (2020), 103644.

[SK10] Schultz T., Kindlmann G. L.: Superquadric glyphs for symmetric second-order tensors. *IEEE Transactions on Visualization and Computer Graphics 16*, 6 (2010), 1595–1604.

[SK16] Seltzer N., Kindlmann G.: Glyphs for asymmetric second-order 2D tensors. *Computer Graphics Forum 35*, 3 (2016), 141–150.

[SKZ*15] Schöneich M., Kratz A., Zobel V., Scheuermann G., Stommel M., Hotz I.: Tensor lines in engineering: success, failure, and open questions. In *Visualization and Processing of Higher Order Descriptors for Multi-Valued Data*. Springer, 2015, pp. 339–351.

[Slo11] Sloan J.: Carbon fiber market: cautious optimism, 2011.

[SLZZ15] Song W., Liu J., Zhou M., Zheng H.: Fast visualization of stress and strain tensor fields on streamsurfaces with LIC texture. *Journal of Information & Computational Science 12*, 8 (2015), 3207–3219.

[SNY18] Stolarski T., Nakasone Y., Yoshimoto S.: *Engineering Analysis with ANSYS Software*. Butterworth-Heinemann, 2018.

[SSK*14] Schöneich M., Stommel M., Kratz A., Zobel V., Scheuermann G., Hotz I., Burgeth B.: Optimization strategy for the design of ribbed plastic components. *Journal of Plastics Technology 04* (2014), 160–175.

[SSSSW13] Schultz T., Schlaffke L., Schölkopf B., Schmidt-Wilcke T.: HiFiVE: a hilbert space embedding of fiber variability estimates for uncertainty modeling and visualization. *Computer and Graphics Forum 32*, 3 (2013), 121–130.

[THBG12] Tricoche X., Hlawitschka M., Barakat S., Garth C.: Beyond topology: a lagrangian metaphor to visualize the structure of 3D tensor fields. In *New Developments in the Visualization and Processing of Tensor Fields*. Springer, 2012, pp. 93–109.

[TIHN07] Takayama K., Igarashi T., Haraguchi R., Nakazawa K.: A sketch-based interface for modeling myocardial fiber orientation. In *8th Symposium on Smart Graphics* (2007), Butz A., Fisher B., Krüger A., Olicier P., Owada S., (Eds.), pp. 1–9.

[TNCK13] Thorpe S. D., Nagel T., Carroll S. F., Kelly D. J.: Modulating gradients in regulatory signals within mesenchymal stem cell seeded hydrogels: a novel strategy to engineer zonal articular cartilage. *PLoS ONE 8*, 4 (Apr 2013), e60764.

[TNKW20] Teixeira F. S., Neufeld E., Kuster N., Watton P. N.: Modeling intracranial aneurysm stability and growth: an integrative mechanobiological framework for clinical cases. *Biomechanics and Modeling in Mechanobiology* (Jun 2020), 1–19.

[Tri02] Tricoche X.: *Vector and Tensor Field Topology Simplification, Tracking, and Visualization*. PhD thesis, University of Kaiserslautern, 2002.

[TT12] Tape W., Tape C.: A geometric setting for moment tensors. *Geophysical Journal International 190*, 1 (2012), 476–498.

[TT15] Tape W., Tape C.: A uniform parametrization of moment tensors. *Geophysical Journal International 202*, 3 (07 2015), 2074–2081.

[UBG*12] Urbancic T. I., Baig A., Goldstein S. B., et al.: Assessing stimulation of complex natural fractures as characterized using microseismicity: an argument the inclusion of subhorizontal fractures in reservoir models. In *SPE Hydraulic Fracturing Technology Conference* (2012), Society of Petroleum Engineers.

[UBGB10] Urbancic T., Baig A., Guest A., Buckingham K.: HFM: dynamic behavior of fracture networks. In *SEG Microseismic Workshop* (2010).

[Vav14] Vavryčuk V.: Iterative joint inversion for stress and fault orientations from focal mechanisms. *Geophysical Journal International 199*, 1 (2014), 69–77.

[WAL*14] Weissenböck J., Amirkhanov A., Li W., Reh A., Amirkhanov A., Groller E., Kastner J., Heinzl C.: FiberScout: an interactive tool for exploring and analyzing fiber reinforced polymers. In *Visualization Symposium (PacificVis), 2014 IEEE Pacific* (2014), IEEE, pp. 153–160.

[War02] Ward M. O.: A taxonomy of glyph placement strategies for multidimensional data visualization. *Information Visualization 1*, 3-4 (2002), 194–210.

[WAS*18] Weissenböck J., Arikan M., Salaberger D., Kastner J., De Beenhouwer J., Sijbers J., Rauchenzauner S., Raab-Wernig T., Gröller E., Heinzl C.: Comparative visualization of orientation tensors in fiber-reinforced polymers. In *Proceedings of the 8th Conference on Industrial Computed Tomography (iCT 2018), Wels, Austria* (2018), pp. 1–9.

[WAWS17] Wu J., Aage N., Westermann R., Sigmund O.: Infill optimization for additive manufacturing–approaching bone-like porous structures. *IEEE Transactions on Visualization and Computer Graphics 24*, 2 (2017), 1127–1140.

[WB05] Wilson A., Brannon R.: Exploring 2D tensor fields using stress nets. In *VIS 05. IEEE Visualization 2005*, (11 2005), pp. 11–18.

[WBT*14] Walton S., Berger K., Thiyagalingam J., ane Hui Fang B. D., Holloway C., Trefethen A. E., Chen M.: Visualizing cardiovascular magnetic resonance (CMR) imagery: challenges and opportunities. *Progress in Biophysics and Molecular Biology 115* (2014), 349–358.

[WBWD12] Wu J., Bürger K., Westermann R., Dick C.: Interactive residual stress modeling for soft tissue simulation. In *EG Workshop on Visual Computing for Biology and Medicine (VCBM)* (2012), Ropinski T., Ynnerman A., Botha C., Roerdink J., (Eds.).

[WGSC18] Wang R., Gu Y. J., Schultz R., Chen Y.: Faults and non-double-couple components for induced earthquakes. *Geophysical Research Letters 45*, 17 (2018), 8966–8975.

[WH17] Wang B., Hotz I.: Robustness for 2D symmetric tensor field topology. In *Modeling, Analysis, and Visualization of Anisotropy*. Springer, 2017, pp. 3–27.

[Wil93] Willemann R. J.: Cluster analysis of seismic moment tensor orientations. *Geophysical Journal International 115*, 3 (1993), 617–634.

[WK14] Wong J., Kuhl E.: Generating fiber orientation maps in human heart models using Poisson interpolation. *Computer Methods in Biomechanics and Biomedical Engineering 17*, 11 (2014), 1217–1226.

[WLY04] Wünsche B., Lobb R., Young A. A.: The visualization of myocardial strain for the improved analysis of cardiac mechanics. In *Conference on Computer Graphics and Interactive Techniques* (2004).

[Wol93] Wolff J.: Das gesetz der transformation der knochen. *DMW-Deutsche Medizinische Wochenschrift 19*, 47 (1893), 1222–1224.

[WPG*97] Westin C.-F., Peled S., Gudbjartsson H., Kikinis R., Jolesz F. A.: Geometrical diffusion measures for MRI from tensor basis analysis. In *Proceedings of the International Society for Magnetic Resonance Medicine (ISMRM)* (1997), p. 1742.

[Wri08] Wriggers P.: *Nonlinear finite element methods*. Springer Science & Business Media, 2008.

[WWW20] Wang J., Wu J., Westermann R.: A Globally conforming lattice structure for 2D stress tensor visualization. *Computer Graphics Forum 39*, 3 (2020), 417–427.

[WY03] Wünsche B., Young A. A.: The visualization and measurement of left ventricular deformation using finite element models. *Journal of Visual Languages & Computing 14* (2003), 299–326.

[WZL*12] Wang Y., Zhang J., Lehmann D. J., Theisel H., Chi X.: Automating transfer function design with valley cell-based clustering of 2D density plots. *Computer Graphics Forum 31*, 3 (2012).

[YVAB18] Yu C., Vavryčuk V., Adamová P., Bohnhoff M.: Moment tensors of induced microearthquakes in the geysers geothermal reservoir from broadband seismic recordings: Implications for faulting regime, stress tensor, and fluid pressure. *Journal of Geophysical Research: Solid Earth 123*, 10 (2018), 8748–8766.

[ZDL*11] Zhang G., Du S., Lai Y., Ni T., Hu S.: Sketch guided solid texturing. *Graphical Models 73*, 3 (2011), 59–73.

[ZFD*14] Zhang W., Fehrenbach J., Desmaison A., Lobjois V., Ducommun B., Weiss P., Desmaison A.: Structure tensor based analysis of cells and nuclei organization in tissues. *IEEE Transactions on Medical Imaging* (2014).

[ZGZ17] Zhang Y., Gao X., Zhang E.: Applying 2D tensor field topology to solid mechanics simulations. In *Modeling, Analysis, and Visualization of Anisotropy*. Springer, 2017, pp. 29–41.

[ZMD19] Zhao Z., Mu X., Du F.,: Modeling and verification of a new hyperelastic model for rubber-like materials. *Mathematical Problems in Engineering 2019* (2019).

[ZP02] Zheng X., Pang A.: Volume deformation for tensor visualization. In *Proceedings of the conference on Visualization'02* (2002), IEEE Computer Society, pp. 379–386.

[ZP03a] Zheng X., Pang A.: HyperLIC. In *IEEE Visualization*, 2003. VIS 2003 (Oct 2003), pp. 249–256.

[ZP03b] Zheng X., Pang A.: Interaction of light and tensor fields. In *Proceedings of the Symposium on Data visualisation 2003* (2003), Eurographics Association, pp. 157–166.

[ZP04] Zheng X., Pang A.: Topological lines in 3D tensor fields. In *Proceedings of the conference on Visualization'04* (2004), IEEE Computer Society, pp. 313–320.

[ZP05] Zheng X., Pang A.: 2D asymmetric tensor analysis. In *Proceedings of IEEE Visualization 2005* (2005), pp. 3–10.

[ZPP05] Zheng X., Parlett B. N., Pang A.: Topological structures of 3d tensor fields. In *Proceedings of IEEE Visualization 2005* (2005).

[ZRH14] Zobel V., Reininghaus J., Hotz I.: Visualization of two-dimensional symmetric positive definite tensor fields using the heat kernel signature. In *Topological Methods in Data Analysis and Visualization III*. Springer, 2014, pp. 249–262.

[ZRH15] Zobel V., Reininghaus J., Hotz I.: Visualizing symmetric indefinite 2D tensor fields using the heat kernel signature. In *Visualization and Processing of Higher Order Descriptors for Multi-Valued Data*. Springer, 2015, pp. 257–267.

[ZRSZ18] Zhang Y., Roy L., Sharma R., Zhang E.: Maximum number of transition points in 3D linear symmetric tensor fields. In *Conference Proceeding Topology-Based Methods in Visualization* (2018).

[ZS18] Zobel V., Scheuermann G.: Extremal curves and surfaces in symmetric tensor fields. *The Visual Computer 34*, 10 (2018), 1427–1442.

[ZSS15] Zobel V., Stommel M., Scheuermann G.: Feature-based tensor field visualization for fiber reinforced polymers. In *2015 IEEE Scientific Visualization Conference (SciVis)* (2015), IEEE, pp. 49–56.

[ZSS17] Zobel V., Stommel M., Scheuermann G.: Visualizing gradients of stress tensor fields. In *Modeling, Analysis, and Visualization of Anisotropy*. Springer, 2017, pp. 65–81.

[ZTL13] Zou W.-N., Tang C.-X., Lee W.-H.: Identification of symmetry type of linear elastic stiffness tensor in anarbitrarily orientated coordinate system. *International Journal of Solids and Structures 50*, 14-15 (2013), 2457–2467.

[ZTZ15] Zhang Y., Tzeng Y.-J., Zhang E.: Maximum number of degenerate curves in 3D linear tensor fields. In *Topological Methods in Data Analysis and Visualization* (2015), Springer, pp. 221–234.

[ZYZ*19] Zhao Y., Yang T., Zhang P., Xu H., Zhou J., Yu Q.: Method for generating a discrete fracture network from microseismic data and its application in analyzing the permeability of

rock masses: a case study. *Rock Mechanics and Rock Engineering 52*, 9 (2019), 3133–3155.

[ZZ15] Zhang E., Zhang Y.: 3D symmetric tensor fields: what we know and where to go next. In *Topological and Statistical Methods for Complex Data*. Springer, 2015, pp. 111–124.

Supporting Information

Additional supporting information may be found online in the Supporting Information section at the end of the article.

Data S1